All-organic superhydrophobic coatings with mechanochemical robustness and liquid impalement resistance

Chaoyi Peng[1,2], Zhuyang Chen[1], Manish K. Tiwari[1,3]*

[1]Nanoengineered Systems Laboratory, UCL Mechanical Engineering, University College London, London WC1E 7JE, UK

[2]Department of Material Science and Engineering, College of Aerospace Science and Engineering, National University of Defense Technology, Changsha, Hunan, 410073, P. R. China

[3]Wellcome/EPSRC Centre for Interventional and Surgical Sciences, University College London, London, UK

Abstract: Superhydrophobicity is a beautiful evolutionary adaption manifested by several natural surfaces. Artificial superhydrophobic coatings with good mechanical robustness, substrate adhesion, and chemicals robustness have been achieved separately. However, a simultaneous demonstration of these features along with resistance to liquid impalement via high speed drop/jet impact is challenging. Here, we introduce all-organic, flexible superhydrophobic nanocomposite coatings that can be applied through scalable techniques, e.g. spraying, brushing, etc., and demonstrate strong mechanical robustness (under cyclic tape peels and Taber abrasion) and sustain exposure to highly corrosive and/or oxidising aqua regia and sodium hydroxide solutions. Additionally, the mechanical flexibility of our coatings enables impalement resistance to high speed drops and turbulent jets at least up to ~35 ms^{-1} and Weber number ~43,000. With multifaceted robustness and scalability, our coatings should find potential usage in harsh chemical engineering as well as infrastructure, transport vehicles and communication equipment.

Confidential

*Corresponding author. Email: m.tiwari@ucl.ac.uk, Phone: +44 20 3108 1056, Fax: +44

(0)20 7388 0180

Superhydrophobicity is an evolutionary adaption manifested by several natural surfaces such as lotus leaves[1], water strider legs[1], butterfly wings[2], etc. wherein extreme water repellency is achieved by exploiting micro/nano-scale or hierarchical surface textures and low surface energy materials. Artificial superhydrophobic materials offer exciting promise for self-cleaning[3], anti-icing[4], anti-fouling[5], energy efficient fluid transport[6], oil-water separation[7], etc. Superhydrophobic materials/coatings[8] with mechanical robustness[9,10], good substrate adhesion[11-13], ability to sustain abrasion via low speed impact of sand particles (speed < 3 ms^{-1})[14], stability to high temperature exposure[15] and good chemical resistance[16,17] have been reported. However, a simultaneous demonstration of these features is a major challenge. For example, the coatings including inorganic nanoparticles or building blocks (e.g. TiO_2[12], SiO_2[14], rare earth oxides[15], etc.) offer mechanical robustness, however, they are chemically susceptible, especially to strong acids and bases. Similarly, organic coatings have good chemical resistance[16,17], but poor mechanical properties. Additionally, and just as importantly, a lack of resistance to liquid impalement into the surface texture via high speed drop/jet impact another important issue, which limits the practical exploitation of superhydrophobic coatings. To exemplify, a moving car or wind turbine blades must withstand high speed water drop impacts and/or sand erosion; equipment in chemical process and sewage treatment plants are exposed to strong acid or base corrosion and may even be exposed to highly oxidising conditions. Even simple infrastructure components exposed to elements can experience impact by high speed water drop. Despite notable progress, superhydrophobic coatings with such characteristics have remained elusive.

For any surface, contact angle θ of a water droplet lying on the surface quantifies its affinity to water; smooth surfaces with $\theta > 90°$ are hydrophobic[18]. On a rough, hydrophobic surface,

Confidential

a droplet can be supported by the solid surface asperities and air. This composite interface – i.e., liquid in contact with the solid asperities and air – enhances hydrophobicity and enables easy drop roll-off on surfaces and the drop is said to attain the so called Cassie-Baxter state[18]. Composite materials comprising micro/nanoscale filler particles dispersed in hydrophobic polymer matrices, have been utilised to achieve superhydrophobicity[19]. However, multi-pronged robustness focused on herein, remains a challenge.

Robustness strategy

There are three different, and at times synergistic, strategies that can be exploited to address these challenges and obtain a robust coating. Firstly, just as in living systems, we can exploit feature of easy repair ability and self-healing[20-22]. This naturally helps overcome the issue of mechanical damage, introduced, for example, by abrasion. Secondly, we can design coatings that fail in a self-similar manner, such that upon damage the exposed parts of coatings are similar in texture and functionality to the top/undamaged layer. Thirdly, if these coatings are compliant, then they can soften the peak pressure generated during impact of a droplet or a jet on them. Here, we exploit a combination of the latter two strategies and introduce a multi-fluorination strategy (**Fig. 1**) in order to formulate all-organic nanocomposite coatings comprising of fluorinated epoxy resin, perfluoropolyether and fluoropolymeric nanoparticles as their building blocks. The epoxy resin is selected due to its mechanical and chemical robustness, ability to disperse nanoparticles through hydrophilic functional groups (Fig. 1a) and strong substrate adhesion; the perfluoropolyether helps tune the surface energy and flexibility; and the fluoropolymer nanoparticles offer the texture control and low surface energy. The rational choice of all the constituents in our all-organic formulation also imparts excellent chemical robustness to our coatings.

Rational multi-fluorination

The multi-fluorination was achieved as follows. First, fluorinated amine curing agent was synthesized by reacting diethylenetriamine and heptafluorobutyric acid fluoropolymers (Supplementary Methods, Supplementary Figure 1). Then, this fluorinated amine was used to connect (graft) the epoxy backbone with low surface energy fluoropolymers in order to obtain fluorinated epoxy resin (Fig. 1b, denoted as FE resin). Second, a perfluoropolyether (Krytox® oil) was blended with the FE resin to further enhance the hydrophobicity (Fig. 1c, denoted as KFE resin) and to introduce mechanical flexibility. Simple epoxy resins can be hard, which is not beneficial for liquid impact resistance (see below). Thus the addition of perfluoropolyether was crucial to realisation of superhydrophobic coatings with low hysteresis and easy drop roll-off. Third, polytetrafluoroethylene (PTFE) nanoparticles were incorporated into the KFE resin to obtain the superhydrophobic nanocomposite coating (Fig. 1d, denoted as PKFE coating). For dynamic wettability characterisation of the coatings, water drop advancing and receding contact angles, denoted respectively by θ_A and θ_R, and their difference (i.e. contact angle hysteresis, $\Delta\theta$) were measured[23]. The initial mean θ_A and $\Delta\theta$ for PKFE were ~158° and 3°, respectively, and these values remained stable after 6 months of storage in room conditions.

Fourier transform infrared (FTIR) spectroscopy was used to assess the compositions (Fig. 1e). The peaks at ~550-650 cm^{-1} and ~1150-1250 cm^{-1} confirm the presence of –CF$_2$ and –CF$_3$ functional groups[24], which proves the successful fluorination of the epoxy resin via grafting, blending and mixing (i.e. all the different steps in our multi-fluorination strategy). For coating preparation, the multi-fluorination was realised via wet processing to realise a

stable polymer/particle suspension of the epoxy resin, the fluorinated amine (curing agent), the perfluoropolyether, the PTFE nanoparticles and an organic solvent (see Methods and Supplementary Methods. The resulting suspension could be sprayed, brushed or roll coated on nearly any substrates such as glass, metal, paper, carbon fibre composites, etc. (Supplementary Methods, Supplementary Figure 2). As a final step the coatings were annealed in air at ~100 °C for ~1 hour (Supplementary Figure 3). The entire coatings preparation is scalable to large area substrates (Supplementary Figure 2). Note that we introduce fluorination through the amine hardener for the epoxy, in aqueous synthesis conditions and, crucially, at room temperature. Therefore, our grafting technique is safe, quick and easy to perform, without involving any toxic organic solvents or byproducts. Water is our only synthesis byproduct from epoxy fluorination and just needs to be evaporated at 100 °C; the approach is safe and environment friendly.

A series of robustness tests were employed to probe the mechanical, chemical and droplet/jet impact resistance of the PKFE nanocomposite coatings. The following results were all obtained using the coating with an optimal ~75 wt.% loading of PTFE nanoparticles, which was determined by preparing a series of coatings with different nanoparticle loadings (Supplementary Note 1) and testing liquid repellency (Supplementary Figure 4) and abrasion resistance (Supplementary Figure 5).

Mechanical robustness

Mechanical robustness is the major challenge for superhydrophobic coatings and was thus considered first. Results of two different types of mechanical robustness tests are presented in **Fig. 2**. First, a high tack tape (VHB, 3M, with an adhesion to steel value of 2,600 Nm^{-1}) was

used for tape peel (adhesion) test (Fig. 2a and Supplementary Note 2). Repetitive tape application and peel off cycles were used to assess the coating degradation (Supplementary Figure 6) – single peel off did not affect the drop contact and sliding angles, providing a first indication of the coating robustness. Ten peel off cycles caused a slight drop in θ_A, from 158° to ~155° and a slight increase of hysteresis ($\Delta\theta$) from 3° to 4° (see Fig. 2b). However, the coating maintained excellent water repellency even after 30 tape peel off cycles (Fig. 2b); this is also evident from virtually no change in coating morphology (see Fig. 2e and 2f, respectively for fresh and tape peeled coatings) and the complete bouncing of a water drop impacting at ~0.22 ms^{-1} (Fig. 2h, cases 1 and 2). We also performed cross hatch, ASTM standard adhesion test using two different tapes: a standard Elcometer 99 (adhesion to steel: 642 Nm^{-1}) and the high tack VHB tape. The Elcometer 99 tape did not remove any coatings, whereas none or less than 5% of the coating was removed on to the VHB tape (see Supplementary Note 2 and Supplementary Figures 6c and 6d) and ~10 μl water drops easily rolled off the tested area at inclination angles of less than 5°.

As a second mechanical robustness test, the abrasion resistance of the coatings was tested next using ASTM standard Taber abrasion technique (Supplementary Note 3), where loaded wheels are abraded against coated substrates, mounted on a rotary platform (see Fig. 2c and Supplementary Figure 7). The change in the coating θ_A and thickness with the Taber abrasion cycles are plotted in Fig. 2d for three different loads. Each abrasion data point and error bar (e.g. in Fig. 2c, Supplementary Figures 5 and 14) was obtained from distinct measurements on 3 different coating samples and at least at 3 different locations on each. After 100 abrasion cycles, the θ_A of PKFE coating remained above 150° for loads of 150 g and 200 g and reduced to ~146° for 250 g (Fig. 2d). This clarifies the progressively higher abrasion rate with increased abrasion loads. Note that in each case $\Delta\theta$ remained under 10°.

We attribute the above abrasion resistant water repellency to our multi-fluorination strategy, which enables the PKFE nanocomposite coatings to maintain their texture even while being degraded by abrasion. At sufficient abrasion strength (250 g load), the degradation after 100 cycles was severe enough (see Fig. 2g) to result in the loss of the resistance to impalement by an impacting drop impacting. However, a complete drop bounce off and impalement resistance was maintained at 200 g load (see Fig 2h, case 3), even after 100 abrasion cycles. The case 4 in Fig. 2h shows drop rebounding from the region of the coating subjected to high speed jet impact, which will be discussed later. In course of determining the optimal particle loading, the effect of constituent concentration on abrasion resistance was also investigated thoroughly in order to determine the optimal concentration of the PTFE particles and epoxy resin (see Supplementary Note 1 and Supplementary Figure 5).

Chemical robustness

Our all-organic formulation was also developed with chemical robustness in mind. Thus, to assess harsh chemical corrosion resistance, we used aqua regia (a mixture of highly concentrated hydrochloric acid (HCl) and nitric acid (HNO$_3$) in 3:1volume ratio) – a strongly acidic and very potent oxidising agent – and 1M basic, sodium hydroxide (NaOH) solution. Although such extreme harsh chemical corrosion is not very common in practice, it is a meaningful means to establish the coating chemical robustness. The tests were performed by dipping the coated glass slides into the chemical solutions and periodically removing the samples and measuring the θ_A and $\Delta\theta$ after water rinsing and drying. The results are shown in **Fig. 3**. The coating maintained a θ_A of greater than 150° after 60 min of aqua regia immersion (Fig. 3a) and 12 hours of 1M NaOH exposure (Fig. 3b); within experimental error the $\Delta\theta$ of ~10° or lower is also maintained. SEM images (Fig. 3c and 3d) show no observable

Confidential

damage. The reason for such excellent chemical resistance is the inherent chemical inertness of our rationally selected the PKFE nanocomposite constituents.

Liquid impalement resistance

Resistance to impalement by high speed water drops and jets was considered next; the results are summarised in **Fig. 4**. Supplementary Movie 1 shows water drop impacts at ~1.0 ms^{-1}, ~2.0 ms^{-1} and ~4.6 ms^{-1} obtained by free fall of droplets; the droplet at 4.6 ms^{-1} atomizes upon impact. The important time instants during the impact are captured in Supplementary Figure 8 in Supplementary Note 4. Clearly, at the high impact speed, the droplet and its fragments spent much less time on the surface (for example, Fig. 4a showing 8.0 ms as opposed to ~15.3 ms for 4.6 ms^{-1}, see Supplementary Figure 8 and Supplementary Movie 1). This contact time reduction is due to drop atomization (splashing) upon impact at relatively high liquid Weber number $(We_l) = \rho_l V^2 d/\gamma_{LG}$, with ρ_l denoting the liquid density, γ_{LG} the liquid-gas interfacial tension, V the impact speed and d the characteristic length scale, taken as the diameter for both the jet and drops in this study (the We_l values are shown in the Supplementary Movies). The splashing-led reduction in contact time observed here at high We_l is distinct from the reduction in contact time through surface texturing[25,26] or the observed scaling of the contact time with drop resonance time scale[26,27], both of which have been obtained through impact studies at low We_l (typically $<10^2$). Note that unlike a few previous studies on drop splashing on superhydrophobic surface (e.g. Tsai *et al.*[28]), on PKFE coatings after drop impact and splashing, we observed no signs of liquid impalement into the surface texture. Impaled liquid is typically visible as either tiny remnant droplet[29] or as liquid patch in post-impact top view photographs[28].

Confidential

To investigate higher speed impacts, water jets were generated using pneumatic forcing of water through nozzles (see Supplementary Note 5 and Supplementary Figure 9); this helped overcome the limitation of maximum reachable velocity (terminal velocity) for gravity accelerated drops[23]. The jet velocity measurements is described in Supplementary Note 5 (Supplementary Figure 10). Supplementary Movies 2 and 3 show impact of continuous water jets of 0.25 mm and 2.5 mm diameter, respectively. The corresponding We_l values are also shown in the movies and the jets are classified in different regime based on the jet flow parameters and material properties. The finer jets (0.25 mm diameter) atomize upon substrate impact at high speeds, while the larger jet forms a stagnation point at the point of impact and follows the axisymmetric stagnation flow trajectory as marked by the blue dotted line in Fig. 4b as a simple guide to the eye. We also tested the ability to the PKFE coatings to withstand repeated jet impact events by subjecting them 20 times to 0.25 mm jet at 25 ms^{-1}, for ~10 s each time. No damage was incurred. The coatings were also tested with impact of jets on surfaces inclined at 45° (see Supplementary Movies 4 and 5 for jets with 0.25 and 2.5 mm diameter, respectively). Additionally, we tested the impalement resistance of the PKFE coating up to ~35 ms^{-1} using 2.5 mm jet (see Supplementary Figure 11 and Supplementary Movie 6), with We_l ~43,000; this was at upper limit of velocity achievable in our setup and is We_l 4-10 times higher than recent prior works[30,31]. Post-impact θ_A measurements (Fig. 4c shows a still image of droplet on the PKFE surface after jet impact test) and morphology (Fig. 4d) showed no observable damage. The low speed drop impact resulted in complete droplet bounce off on the surface and the measured restitution coefficient remained at ~0.9 before and after jet impact (see Supplementary Figure 12 and Supplementary Note 5).

The PKFE coatings are flexible; the flexibility is demonstrated in Supplementary Movie 7. The flexibility arises due to homogenous blending of the fluorinated epoxy with

perfluoropolyether (Krytox) and soft PTFE nanoparticles. The softness of these coatings is in fact beneficial for impalement resistance. During impact of a droplet or a jet on a substrate, the impalement of liquid meniscus into surface texture is primarily influenced by transient peak in water hammer pressure (P_{wh}), which depends on acoustic impedance of the drop/substrate combination (Supplementary Note 6, see Supplementary Figure 13). Typically, for a rigid substrate the effective acoustic impedance can be approximated as equal to that of water. However, on soft and flexible coatings, such as the one presented herein (see Supplementary Note 6 and the region highlighted 'Flexible coatings' in Supplementary Figure 13), the overall acoustic impedance can be as much as 25% lower – for typical material property values – with corresponding reduction in the peak P_{wh}. This is a major advantage and, at least partially, helps explain the excellent liquid impalement resistance demonstrated by the PKFE coatings. Note that despite use of perfluoropolyether (i.e. Krytox® 1506 oil), our soft coating formulation is different from the recently proposed immiscible oil infused textured surfaces for liquid repellency[32]. For oil infused surfaces, immiscibility of the water with the oil (e.g. Krytox) is exploited to achieve low $\Delta\theta$; however, the adhesion of water drops on oil infused surfaces and the drop roll-off speed is controlled by the oil viscosity[33]. In fact, the drop roll-off on our coatings is faster than the Krytox oil infused surfaces. This is captured in Supplementary Movie 8, where we infused part of our coatings with the oil, after coating preparation and curing (see also Supplementary Note 7). Clearly the Krytox infused (wet) part has much higher drop adhesion. Therefore, our strategy to blend Krytox in the coatings formulation rather than infusing the Krytox on a micro/nanotextured substrate has a clear advantage.

Comparative robustness assessment

Confidential

We also compared our PKFE coatings with four different state-of-the-art coatings to establish the superiority of their robustness (see Supplementary Note 8 and Supplementary Figure 14). The comparative results show that PKFE coatings is about four times better in terms tape peel resistance, a factor of two better in abrasion resistance and possess nearly an order of magnitude better chemical resistance and resistance to high speed liquid impact (measured using We_l). Additionally, the fluorinated components in PKFE are rationally selected to have minimal environmental impact: perfluoroalkane functionalised epoxy, PTFE and Krytox are all stable and un-reactive (see Fig. 3).

In summary, we demonstrated a robust all-organic nanocomposite coating that sustained water repellency under a variety of ultra-harsh mechanical and chemical environments – this included impressive features such as an ability to resist liquid impalement during impact of 2.5-mm diameter water jet at ~35 ms^{-1} (i.e. 126 km/h), and sustaining exposure to aqua regia corrosion. The robustness of our coatings emerges from their flexibility and an ability to retain superhydrophobicity through a layer by layer material removal when subjected to mechanical abrasion. The flexibility enables a cushioning of pressure peaks during impact of liquid drops and jets, thereby helping to achieve excellent liquid impalement resistance and, in addition, a rational choice of all-organic components enables good chemical robustness. The robustness of our all-organic PKFE nanocomposite coatings – prepared mostly using off the shelf constituents – will expand the application scope of superhydrophobic coatings.

Reference

1   Feng, X. J. & Jiang, L. Design and creation of superwetting/antiwetting surfaces. *Adv. Mater.* **18**, 3063-3078, doi:10.1002/adma.200501961 (2006).

2   Zheng, Y., Gao, X. & Jiang, L. Directional adhesion of superhydrophobic butterfly wings. *Soft Matter* **3**, 178-182, doi:10.1039/b612667g (2007).

3   Blossey, R. Self-cleaning surfaces — virtual realities. *Nat. Mater.* **2**, 6 (2003).

4   Jung, S., Tiwari, M. K., Doan, N. V. & Poulikakos, D. Mechanism of supercooled droplet freezing on surfaces. *Nat. Commun.* **3**, 615, doi:10.1038/ncomms1630 (2012).

5   Genzer, J. & Efimenko, K. Recent developments in superhydrophobic surfaces and their relevance to marine fouling: a review. *Biofouling* **22**, 339-360, doi:10.1080/08927010600980223 (2006).

6   Cottin-Bizonne, C., Barrat, J. L., Bocquet, L. & Charlaix, E. Low-friction flows of liquid at nanopatterned interfaces. *Nat. Mater.* **2**, 237-240, doi:10.1038/nmat857 (2003).

7   Xue, Z. *et al.* A novel superhydrophilic and underwater superoleophobic hydrogel-coated mesh for oil/water separation. *Adv. Mater.* **23**, 4270-4273, doi:10.1002/adma.201102616 (2011).

8   Darmanin, T., Taffin de Givenchy, E., Amigoni, S. & Guittard, F. Superhydrophobic surfaces by electrochemical processes. *Adv. Mater.* **25**, 1378-1394, doi:10.1002/adma.201204300 (2013).

9   Tesler, A. B. *et al.* Extremely durable biofouling-resistant metallic surfaces based on electrodeposited nanoporous tungstite films on steel. *Nat. Commun.* **6**, 8649, doi:10.1038/ncomms9649 (2015).

10   Mates, J. E., Bayer, I. S., Palumbo, J. M., Carroll, P. J. & Megaridis, C. M. Extremely stretchable and conductive water-repellent coatings for low-cost ultra-flexible electronics. *Nat. Commun.* **6**, 8874, doi:10.1038/ncomms9874 (2015).

11   Yang, H. *et al.* Lotus leaf inspired robust superhydrophobic coating from strawberry-like Janus particles. *NPG Asia Mater.* **7**, e176, doi:10.1038/am.2015.33 (2015).

12   Lu, Y. *et al.* Robust self-cleaning surfaces that function when exposed to either air or oil. *Science* **347**, 1132-1135, doi:10.1126/science.aaa0946 (2015).

13   Steele, A., Bayer, I. & Loth, E. Adhesion strength and superhydrophobicity of polyurethane/organoclay nanocomposite coatings. *J. Appl. Poym. Sci.* **125**, E445-E452, doi:10.1002/app.36312 (2012).

14   Deng, X., Mammen, L., Butt, H.-J. & Vollmer, D. Candle soot as a template for a transparent robust superamphiphobic coating. *Science* **335**, 5 (2012).

15   Azimi, G., Dhiman, R., Kwon, H. M., Paxson, A. T. & Varanasi, K. K. Hydrophobicity of rare-earth oxide ceramics. *Nat. Mater.* **12**, 315-320, doi:10.1038/nmat3545 (2013).

16   Feng, L. *et al.* Superhydrophobicity of nanostructured carbon films in a wide range of pH values. *Ange. Chem.* **115**, 4349-4352, doi:10.1002/ange.200351539 (2003).

17   Wang, C.-F. *et al.* Stable superhydrophobic polybenzoxazine surfaces over a wide pH range. *Langmuir* **22**, 4 (2006).

18   Lafuma, A. & Quere, D. Superhydrophobic states. *Nat. Mater.* **2**, 457-460, doi:10.1038/nmat924 (2003).

19   Tiwari, M. K., Bayer, I. S., Jursich, G. M., Schutzius, T. M. & Megaridis, C. M. Highly liquid-repellent, large-area, nanostructured poly(vinylidene fluoride)/poly(ethyl 2-cyanoacrylate) composite coatings: particle filler effects. *ACS Appl. Mater. Inter.* **2**, 1114-1119, doi:10.1021/am900894n (2010).

20   Neinhuis, C., Koch, K. & Barthlott, W. Movement and regeneration of epicuticular waxes through plant cuticles. *Planta* **213**, 427-434, doi:10.1007/s004250100530 (2001).

21   Li, Y., Li, L. & Sun, J. Q. Bioinspired Self-Healing Superhydrophobic Coatings. *Angewandte Chemie-International Edition* **49**, 6129-6133, doi:10.1002/anie.201001258 (2010).

22   Ahn, B. K., Lee, D. W., Israelachvili, J. N. & Waite, J. H. Surface-initiated self-healing of polymers in aqueous media. *Nat. Mater.* **13**, 867-872, doi:10.1038/nmat4037 (2014).

23   Asthana, A., Maitra, T., Buchel, R., Tiwari, M. K. & Poulikakos, D. Multifunctional superhydrophobic polymer/carbon nanocomposites: graphene, carbon nanotubes, or carbon black? *ACS Appl. Mater. Inter.* **6**, 8859-8867, doi:10.1021/am501649w (2014).

24   Das, I. & De, G. Zirconia based superhydrophobic coatings on cotton fabrics exhibiting excellent durability for versatile use. *Sci. Rep.* **5**, doi:10.1038/srep18503 (2015).

25   Bird, J. C., Dhiman, R., Kwon, H. M. & Varanasi, K. K. Reducing the contact time of a bouncing drop. *Nature* **503**, 385-+, doi:10.1038/nature12740 (2013).

26   Liu, Y. H. *et al.* Pancake bouncing on superhydrophobic surfaces. *Nat. Phys.* **10**, 515-519, doi:10.1038/nphys2980 (2014).

27   Richard, D., Clanet, C. & Quere, D. Surface phenomena: Contact time of a bouncing drop. *Nature* **417**, 811-811, doi:10.1038/417811a (2002).

28   Tsai, P. C., van der Veen, R. C. A., van de Raa, M. & Lohse, D. How micropatterns and air pressure affect splashing on surfaces. *Langmuir* **26**, 16090-16095, doi:10.1021/la102330e (2010).

29   Maitra, T. *et al.* On the nanoengineering of superhydrophobic and impalement resistant surface textures below the freezing temperature. *Nano Lett.* **14**, 172-182, doi:10.1021/nl4037092 (2014).

30   Ellinas, K., Chatzipetrou, M., Zergioti, I., Tserepi, A. & Gogolides, E. Superamphiphobic polymeric surfaces sustaining ultrahigh impact pressures of aqueous high- and low-surface-tension mixtures, tested with laser-induced forward transfer of drops. *Adv. Mater.* **27**, 2231-2235, doi:10.1002/adma.201405855 (2015).

31   Maitra, T. *et al.* Superhydrophobicity vs. ice adhesion: The quandary of robust icephobic surface design. *Adv. Mater. Inter.* **2**, 330-330 (2015).

32   Wong, T. S. *et al.* Bioinspired self-repairing slippery surfaces with pressure-stable omniphobicity. *Nature* **477**, 443-447, doi:10.1038/nature10447 (2011).

33   Smith, J. D. *et al.* Droplet mobility on lubricant-impregnated surfaces. *Soft Matter* **9**, 1772-1780, doi:10.1039/c2sm27032c (2013).

Author Contributions

C.P. and M.K.T. conceived the idea of the robust superhydrophobic coatings presented. M.K.T. guided the work. C.P. and M.K.T. planned the experiments. C.P. executed all the experiments, with support from Z.C. on paper revision experiments, jet impact and contact angle measurements and SEM. C.P. and M.K.T. wrote the paper and interpreted the results, with comments from all authors.

Acknowledgement

Competing Financial Interests

MKT is involved in commercialisation efforts for advanced materials based coatings which are being explored by UCL Business.

Methods

Synthesis of fluorinated amine curing agent.

First, 0.01 mol diethylenetriamine (ReagentPlus®, 99%, Sigma-Aldrich, UK) was dissolved in 10 ml deionized water in a 100 ml beaker and stirred at 125 rpm on a magnetic stirrer plate. Separately, 0.01 mol heptafluorobutyric acid (≥99.5% (GC), Sigma-Aldrich, UK) was dissolved in 10 ml deionized water and added drop by drop to the magnetically stirred diethylenetriamine solution. The mixing should initiate fluorination reaction (Supplementary Figure 1a). After adding all the heptafluorobutyric acid solution, the resulting mixture was heated to 100 °C to evaporate all the water and obtain the fluorinated amine (F-amine). The excess heptafluorobutyric acid will lead to further fluorination (Supplementary Figure 1b). The F-amine so obtained was used as a hardener for epoxy curing.

PKFE nanocomposite coating preparation and scalability.

The following steps were used to obtain a stable polymer/nanoparticle dispersion – to achieve multi-fluorination in a single pot – to be used to fabricate the PKFE nanocomposite coating via spraying or other scalable coating application methods. First, 2.0 g of bisphenol A based epoxy (AIRSTONE™ 760E, Dow) was dissolved in 5 ml acetone and, separately, 10.5 g PTFE nanoparticles (free-flowing powder, with mean particle diameter of 260 nm and standard deviation of 54.2 nm, as reported previously[19], Sigma-Aldrich, UK), were dispersed in 30 ml of acetone by vigorous, magnetic stirring at 1000 rpm for 10 min. The PTFE particle amount was altered to evaluate the role of particle loading on the coating properties (see Supplementary Figures 4 and 5). The epoxy solution was then mixed with the PTFE nanoparticles suspension and the mixture was stirred vigorously for 15 min to obtain PTFE/epoxy suspension. Next, 0.3 g of perfluoropolyether (Krytox® 1506 oil, Sigma-Aldrich, UK) was added to PTFE/epoxy suspension. The mixture was stirred magnetically for

20 min at 1000 rpm, then sonicated in an ultrasonic bath for 15 min at room temperature followed by stirring again for 10 min to obtain a PTFE/Krytox/epoxy dispersion that was highly stable and could be stored in sealed glass bottles at room temperature for more than one month.

Before coating preparation, 1.5 g of F-amine, synthesized as described above, was dissolved in 10 ml acetone by stirring magnetically for 5 min at 300 rpm. The F-amine solution was then mixed with the PTFE/Krytox/epoxy suspension. The mixture was stirred for 5 min at 1000 rpm, sonicated for 15 min followed by a final 5 min stirring at 1000 rpm to obtain a well dispersed PTFE/Krytox/epoxy/F-amine suspension ready to be applied on substrates (e.g., glass, metal, plastics, polymer composite materials, etc.) through any of common large area coating techniques such as spraying, brushing or rolling (Supplementary Figure 2). We tested the superhydrophobicity of PKFE coatings via θ_A and $\Delta\theta$ measurements through all these application methods; however, for ease of quick sample preparation most of the coating samples were prepared by spraying. After applying onto the substrate, in each case, as a final step the coatings were annealed in air at ~100 °C for ~1 hour to remove all the solvents and complete the epoxy curing (see the hardening mechanism in Supplementary Figure 3).

Tape peel test.

A strong bonding tape (VHB, 3M, with adhesion to steel value of 2,600 Nm^{-1}) was used to test the coatings adhesion. The tape was applied by rolling a 4 kg steel roller on the tape twice (Supplementary Figure 6), followed by waiting for 90 seconds and then peeling off – the tape application and peel off comprised one cycle. The process was repeated with advancing and receding contact angle measurements following each cycle (see Fig. 2 and Supplementary Figure 6b). A fresh piece of tape was used for each peel off cycle.

For ASTM (D3359-17) tape tests, cross hatch engravings were created on the coatings at 2 mm spacing using a sharp razor blade, followed by tape application using the 4 kg steel roller and peel off (see Supplementary Figure 6c). After tape application, following the ASTM standard, we waited 90 seconds before peel off. These cross hatch adhesion tests were performed using Elcometer 99 tape (adhesion to steel: 642 Nm^{-1}) and the VHB tape. In each case, following tape peel off, water droplet roll-off was assessed placing a ~10 µl drop on the tested region and gradually tilting the coated sample.

Taber abrasion test.

Abrasion tests were performed following ASTM D4060, using a Taber abrasion machine (see Fig. 2c and Supplementary Figure 7) at three different loads, 150 g, 200 g, and 250 g. The abrasion test samples comprised of coated 10 cm × 10 cm glass plates. Following the ASTM standard, each rotation of the substrate was counted as one abrasion cycle. The coatings' advancing and receding contact angles as well as thickness were measured as a function of Taber abrasion cycles (see Fig. 2d). Any abrasive particles or coating fragments appearing on the samples were rinsed off before measuring thickness and the contact angles.

Droplet impact test.

The drop impact tests were performed by releasing individual water drops from a certain height to enable gravity led acceleration of the drops and achieve different impact speeds. The droplet impacts on substrates were recorded with a Phantom V411 high-speed camera fitted with a macro lens.

Jet impact test.

Confidential

Maximum attainable drop speed in gravity enabled acceleration is limited by terminal velocity. Thus for higher speed liquid impact tests, we employed water jets. Pneumatic forcing of liquid through nozzles of different diameter was used to obtain stable and controllable water jets with high speed (see Supplementary Figure 9). A high pressure nitrogen gas cylinder connected to an electronic pressure valve was used to force water through a nozzle connected to a piston (a needle/syringe assembly). The accuracy of electronic pressure valve was 0.1 bar. Different water jet velocities were obtained by tuning the gas pressure. The electronic pressure valve limited the back pressure on the piston to a maximum of 11 bar. Two different nozzles with nominal diameter of 0.25 mm and 2.5 mm were used; the jet diameters were same as the nozzles. Due to system transients, upon application of pressure control signal on the electronic control valve, the gas back pressure on the piston inside the syringe is expected to ramp up to 11 bar. This transient process caused a time dependent rise in jet speed before levelling off to a steady rate corresponding to the maximum applied pressure. To unravel this transience, we recorded the motion of the piston/water interface inside the cylinder during typical jet impact process using the high speed camera. The motion of the piston could be used to determine the jet speeds through simple mass conservation and knowledge of cylinder and nozzle diameters (see Supplementary Note 5 and Supplementary Figure 10).

Preparation of the commercial and Capstone-CB coatings.

For the comparative tests of PKFE against sprayable coatings from commercial sources and open literature, four different coatings were prepared (see Supplementary Information and Supplementary Figure 14). Capstone-CB is a nanocomposite coating comprising of carbon black (CB) nanoparticles dispersed in a fluoroacrylic copolymer (Capstone ST-100® from DuPont), with equal weight fractions of CB and Capstone[23]. The three different commercial

Confidential

coatings in our comparison were: NTT-AT HIREC 450, Ultra-Ever Dry and NeverWet, which were all prepared by spraying, in accordance with the suppliers' guidance notes. Ultra-Ever Dry and NeverWet are two-part coatings, i.e., they use a primer for adhesion improvement. This is in contrast to PKFE, Capstone-CB and HIREC 450, which are each a one part sprayable formulation.
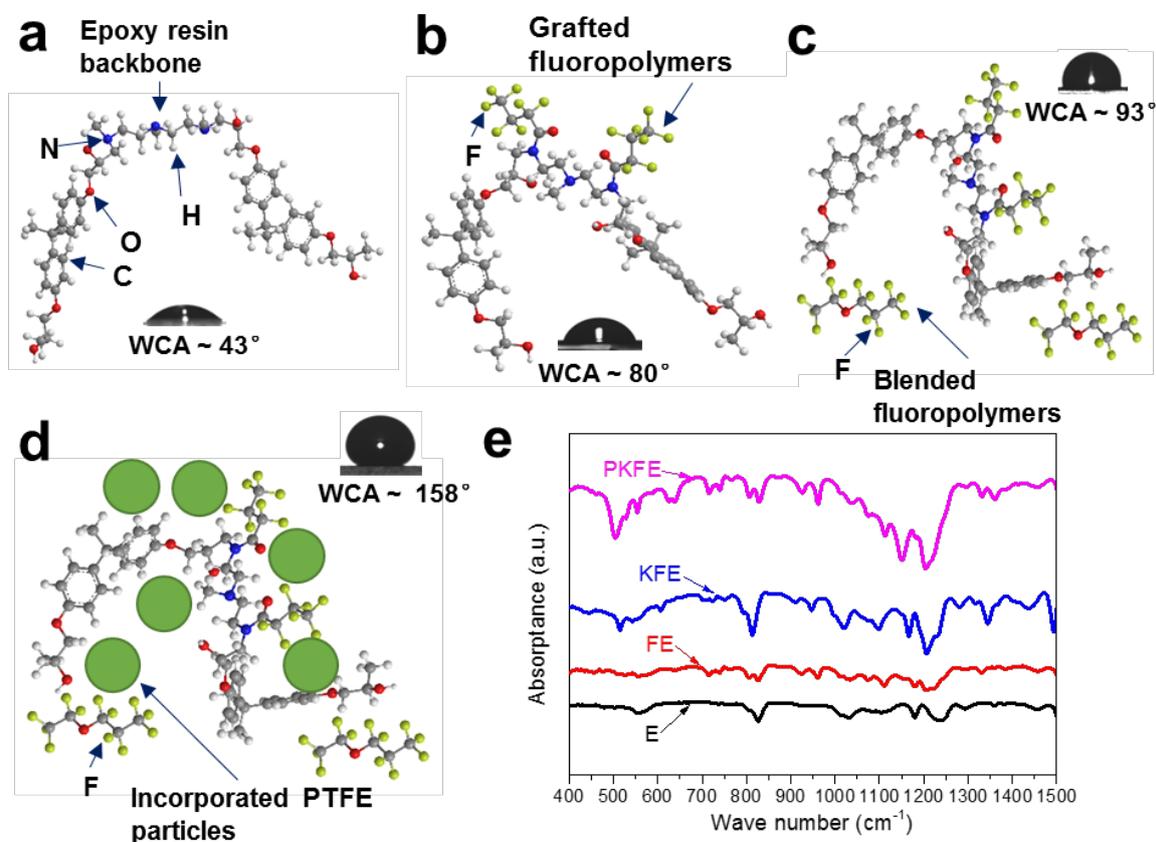
Data availability.

The data sets generated during the current study are available from the corresponding author upon reasonable request.

Code availability.

The Matlab® scripts used to calculate the drop velocities (in Supplementary Note 5) and the contact angle measurements are available from the corresponding author upon reasonable request.

Figures

Figure 1 | Illustration of multi-fluorination strategy for all-organic nanocomposite coating. a, Epoxy resin before fluorination, with water contact angle (WCA) ~43°. **b**, Fluoropolymer grafted epoxy resin (denoted as FE resin), WCA increased to ~80°. **c**, Blending fluoropolymer into FER resin (denoted as KFE resin), WCA further increased to ~93°. **d**, Incorporating PTFE particles to obtain nanocomposite coating (denoted as PKFE coating) with WCA of ~158°. **e**, Fourier transform infrared (FTIR) spectroscopy diagram of pure epoxy (E) resin, FE resin, KFE resin and the PKFE coating (all samples for FTIR spectroscopy were hardened and dried at 100 °C for one hour). The peaks at ~550-650 cm^{-1} and ~1150-1250 cm^{-1} confirm the presence of –CF$_2$ and –CF$_3$ functional groups and the successful fluorination at every step.
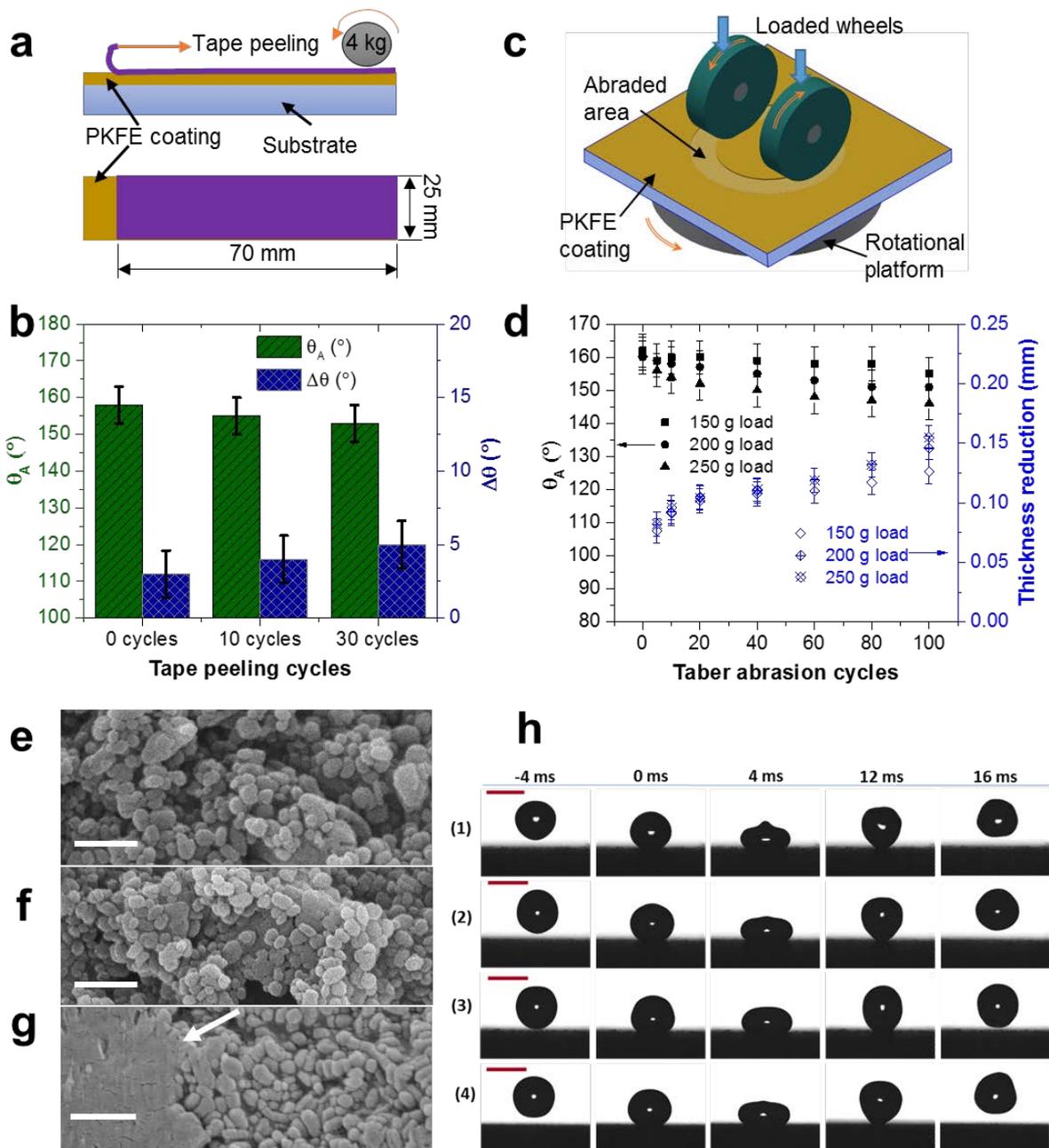
Figure 2 | Mechanical robustness of water repellent PKFE coatings. **a**, Schematic of the tape peel

tests, performed using high tack tape. Tape was applied uniformly by rolling a 4 kg steel roller twice.

b, Effect of tape peel cycles on the water repellency of the PKFE coating – superhydrophobicity is

maintained after 30 cycles (θ_A remained above 155° and $\Delta\theta$ below 5°). **c**, Schematic of mechanical

abrasion tests performed using Taber abrasion tester, comprising loaded abrading wheels rubbing

against coated samples mounted on a rotary platform. **d**, The change in θ_A and the coating thickness

reduction with Taber abrasion cycles with three different abrading loads. θ_A remained ~155° at 150 g

load, ~151° at 200 g and ~146° at 250 g, even after 100 abrasion cycles. **e**, Scanning electron microscope (SEM) image showing PKFE nanocomposite coating morphology featuring PTFE nanoparticles coated with fluorinated epoxy. Scale bar, 1 μm. **f**, SEM image showing the morphology of PKFE coating after 30 tape peel cycles, strong tape peeling caused no observable damage to the coating morphology. Scale bar, 1 μm. **g**, Morphology of the PKFE coating after 100 abrasion cycles of (250 g load); plastic deformation spot (indicated by the arrow) was observed. Scale bar, 1 μm. **h**, A confirmation of coating integrity; complete bounce off shown by water droplets impacting at ~0.22 ms^{-1} on fresh PKFE nanocomposite coating (1), on the coating subjected to 30 tape peel off cycles (2), on the coating after 100 cycles of abrasion at 200 g load (3) and on the coatings after high speed jet impact test (4). Scale bars, 2.5 mm. Error bars were obtained from distinct measurements on 3 different coating samples and at least at 3 different locations on each.
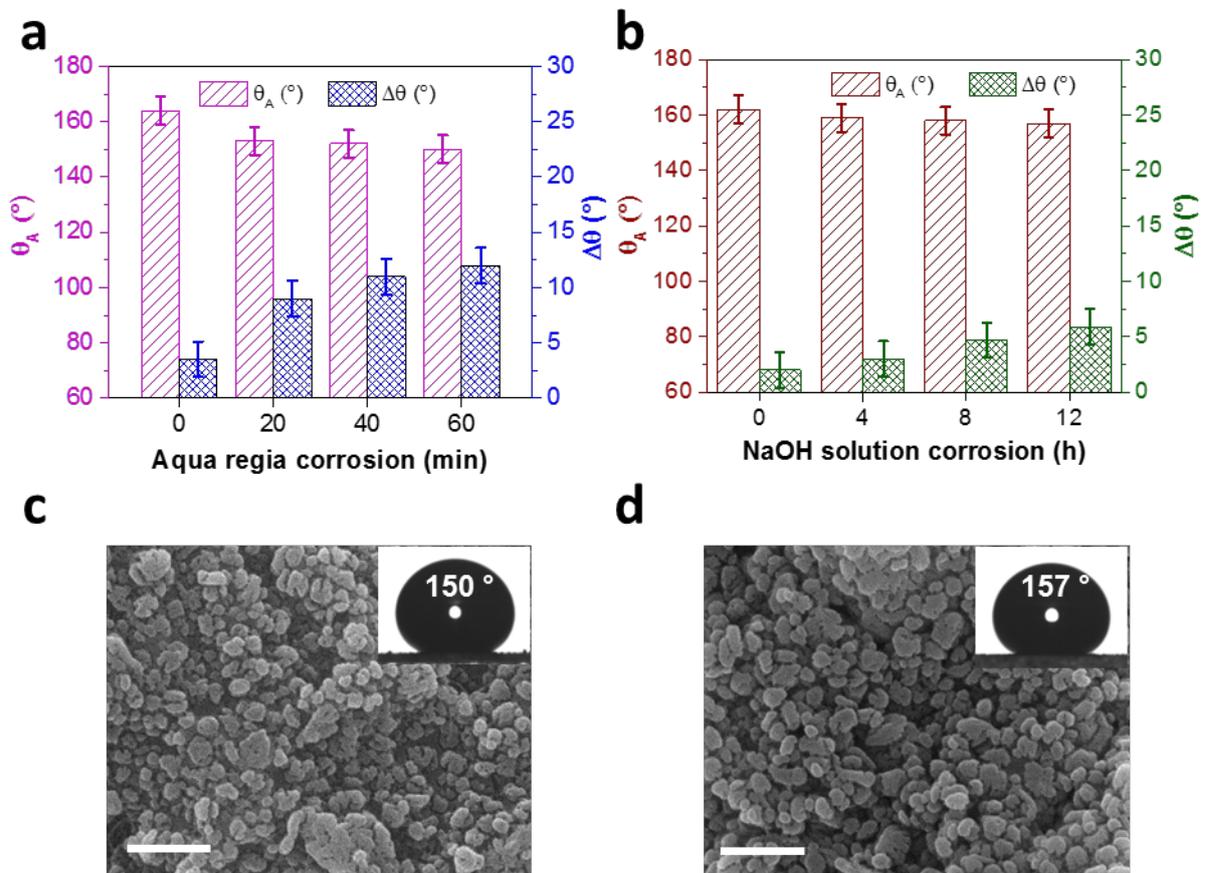
Figure 3 | Chemical resistance of the water repellent PKFE coating. a, Effect of aqua regia corrosion time on the water repellency of the PKFE nanocomposite. θ_A is maintained above 150° after 60 mins. **b**, Effect of NaOH solution (1M) corrosion – the superhydrophobicity is maintained after 12 hours. **c**, Morphology of PKFE coating surface after 60 min in aqua regia corrosion and **d,** after 12 h in 1M NaOH solution. Scale bars, 1 μm. Error bars were obtained from distinct measurements on 3 different coating samples and at least at 3 different locations on each.
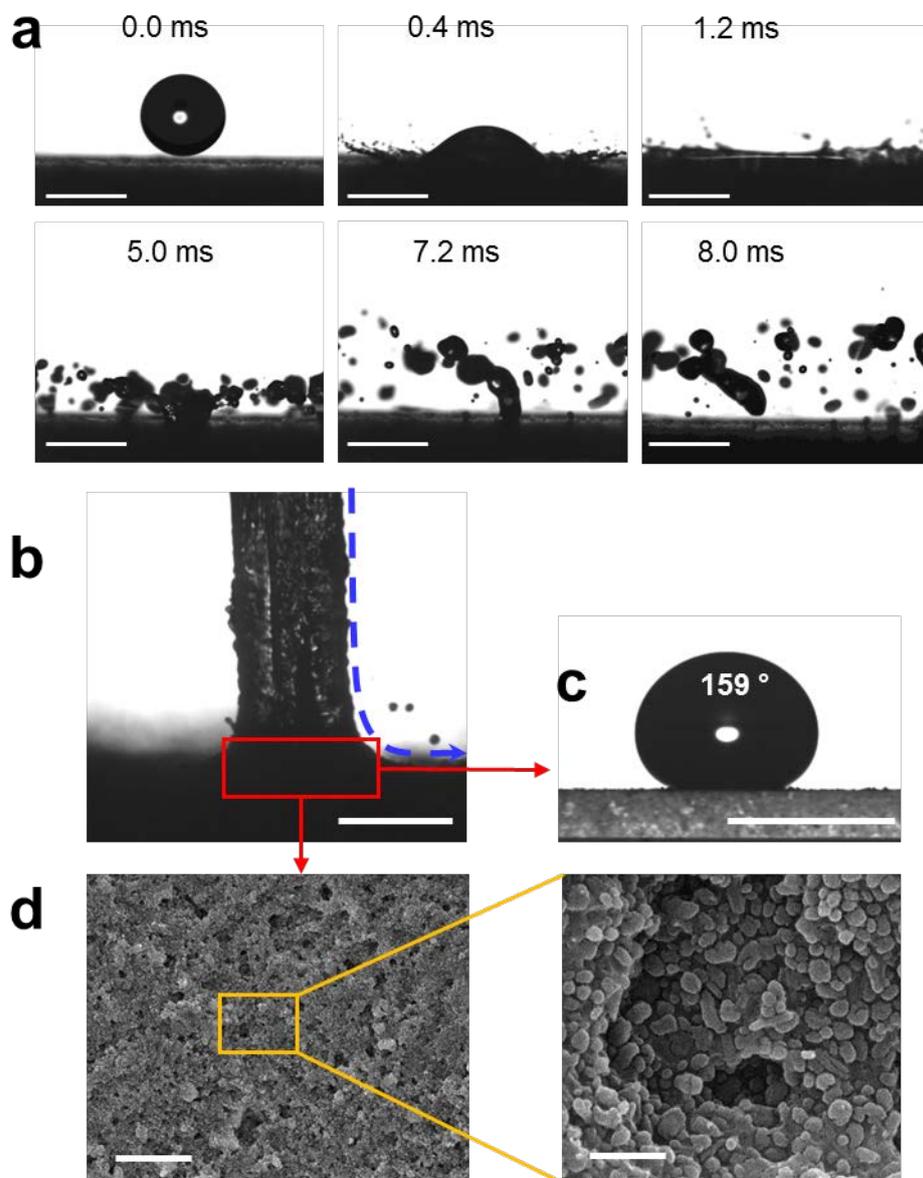
Figure 4 | Robustness of the superhydrophobic PKFE coating upon high speed water droplet and jet impact. a, Water droplet (speed ~4.6 ms^{-1}) atomizing upon impact with the coating, without any signs of impalement into the texture. Scale bar, 2.5 mm. **b**, High speed water jet impacting on the coating with average speed of ~21 ms^{-1} and We_l ~15,000; maximum speed we tested the surfaces at is ~35 ms^{-1} (We_l ~43,000). The coating showed no signs of impalement as tested with drop roll-off angle and restitution coefficient measurements. Scale bar, 2.5 mm. **c**, Water drop on the PKFE surface spot impacted by the water jet in (b). Scale bar, 2.5 mm. **d**, SEM morphology of water jet impacted PKFE surface, showing undamaged rough structure. Scale bars, 10 μm (left) and 1 μm (right).

Supplementary Information

All-organic superhydrophobic coatings with mechanochemical robustness and liquid impalement resistance

Chaoyi Peng[1,2], Zhuyang Chen[1], Manish K. Tiwari[1,3]*

[1]Nanoengineered Systems Laboratory, UCL Mechanical Engineering, University College London, London WC1E 7JE, UK

[2]Department of Material Science and Engineering, College of Aerospace Science and Engineering, National University of Defense Technology, Changsha, Hunan, 410073, P. R. China

[3]Wellcome/EPSRC Centre for Interventional and Surgical Sciences, University College London, London, UK

Supplementary movie captions

Supplementary Movie 1: Water droplets bouncing off the PKFE coating at different velocities. At higher speed, the water droplets atomize upon impact and spend much less time on the substrate compared to the drops impacting at lower speed.

Supplementary Movie 2: Fine water jets (diameter ~0.25 mm) impacting on the PKFE coating vertically with different speeds. The videos show the corresponding jet velocities, and the Weber numbers for liquid ($We_l=\rho_l V^2 d/\gamma_{LG}$) and gas ($We_g=\rho_g V^2 d/\gamma_{LG}$). The jets are indicated as laminar, transitional and turbulent jets based on standard jet atomization thresholds[1]. At low speed we observe a liquid accumulation at the point of impact, without any impalement. At high speeds (> 10 ms^{-1}) the jets atomize upon impacting the substrate.

Supplementary Movie 3: Thick water jets (diameter ~2.5 mm) impacting on the PKFE coating vertically with different speeds. The videos show the corresponding jet velocities, and

the Weber numbers for liquid ($We_l=\rho_l V^2 d/\gamma_{LG}$) and gas ($We_g=\rho_g V^2 d/\gamma_{LG}$). The jets are indicated as laminar, transitional and turbulent jets based on standard jet atomization thresholds[1]. These thick jets do not show atomization at the point of substrate impact, rather a stagnation point flow characterised by axisymmetric bending of incoming jet is observed. However, the liquid did not impale into the coating texture (tested by drop contact and sliding angle measurements at the point of impact) right after jet impact tests.

Supplementary Movie 4: Fine water jets (diameter ~0.25 mm) impacting at different speeds on the PKFE coating inclined at 45°.

Supplementary Movie 5: Thick water jets (diameter ~2.5 mm) impacting at different speeds on the PKFE coating inclined at 45°.

Supplementary Movie 6: A turbulent water jet impacting on the PKFE coating with ~35 ms^{-1}, corresponding to a We_l ~43,000. The video demonstrates the excellent impalement resistance of the nanocomposite coating and its ability to sustain high speed liquid impact. After jet impact test, the left over water droplets from the nozzle bounced or rolled right off from the impact spot. This substantiates the fact that the PKFE coating retains superhydrophobicity after high speed jet impact.

Supplementary Movie 7: Demonstration of good adhesion and mechanical flexibility of the PKFE coatings. PKFE coating on A4 paper maintains superhydrophobicity after rolling, folding and crumpling randomly. Minimum bending radius was less than 2 mm.

Supplementary Movie 8: Water droplets roll-off much faster on the PKFE coating than on the Krytox oil infused PKFE nanocomposite. The mechanical flexibility and low water adhesion are key novel features of our PKFE coatings underpinning their excellent water impalement resistance during high speed impacts.

Supplementary Methods

Amine fluorination.

The dropwise mixing of heptafluorobutyric acid into diethylenetriamine solution should initiate fluorination through reaction of carboxylic group with the amine (Supplementary Figure 1a), which should progress further through heating at 100 °C (see Methods section and Supplementary Figure 1b). The heating also evaporates all the water and produces the fluorinated amine (F-amine) hardener for epoxy curing.
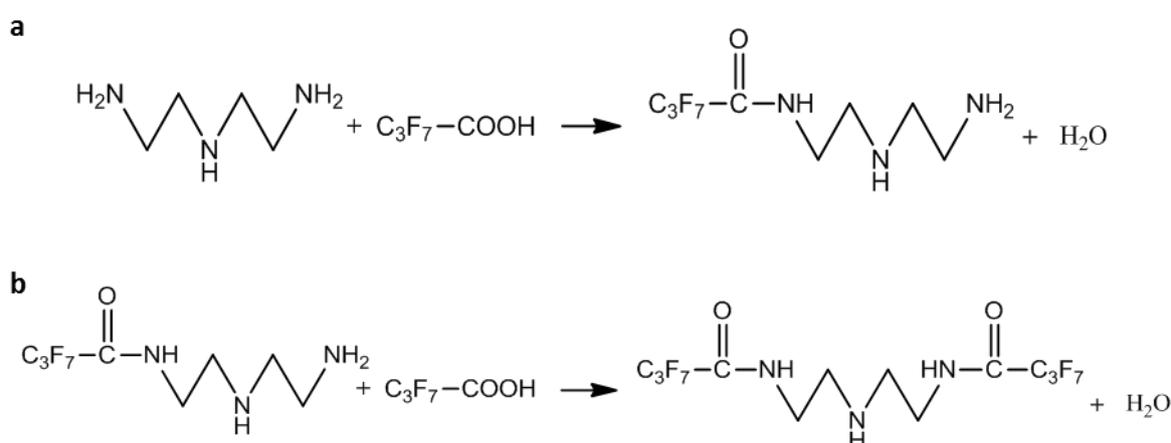

Supplementary Figure 1. Mechanism of fluorinated amine curing agent synthesis. a, Heptafluorobutyric acid reaction with diethylenetriamine. **b**, Excess heptafluorobutyric acid reaction with diethylenetriamine.

Coating preparation and scalability.

Mixture of PTFE/Krytox/epoxy dispersion with F-amine dissolved in acetone (see Methods section of the main paper) was used to prepare the PKFE nanocomposite coatings. This PTFE/Krytox/epoxy/F-amine mixture suspension could be applied on nearly any substrates (e.g., glass, metal, plastics, polymer composite materials, etc.) through any of common large area coating techniques such as spraying, brushing or rolling (Supplementary Figure 2). We tested the superhydrophobicity of the PKFE coatings (via θ_A and $\varDelta\theta$ measurements) obtained

through all these application methods; for ease of quick sample preparation most of the coatings were prepared by spraying. After applying onto the substrate, in each case, as a final step the coatings were annealed (~100 °C for ~1 hour, see Methods) to complete the epoxy curing. The epoxy hardening mechanism is illustrated in Supplementary Figure 3, depicting reaction of epoxide groups with the secondary amines in the F-amine.
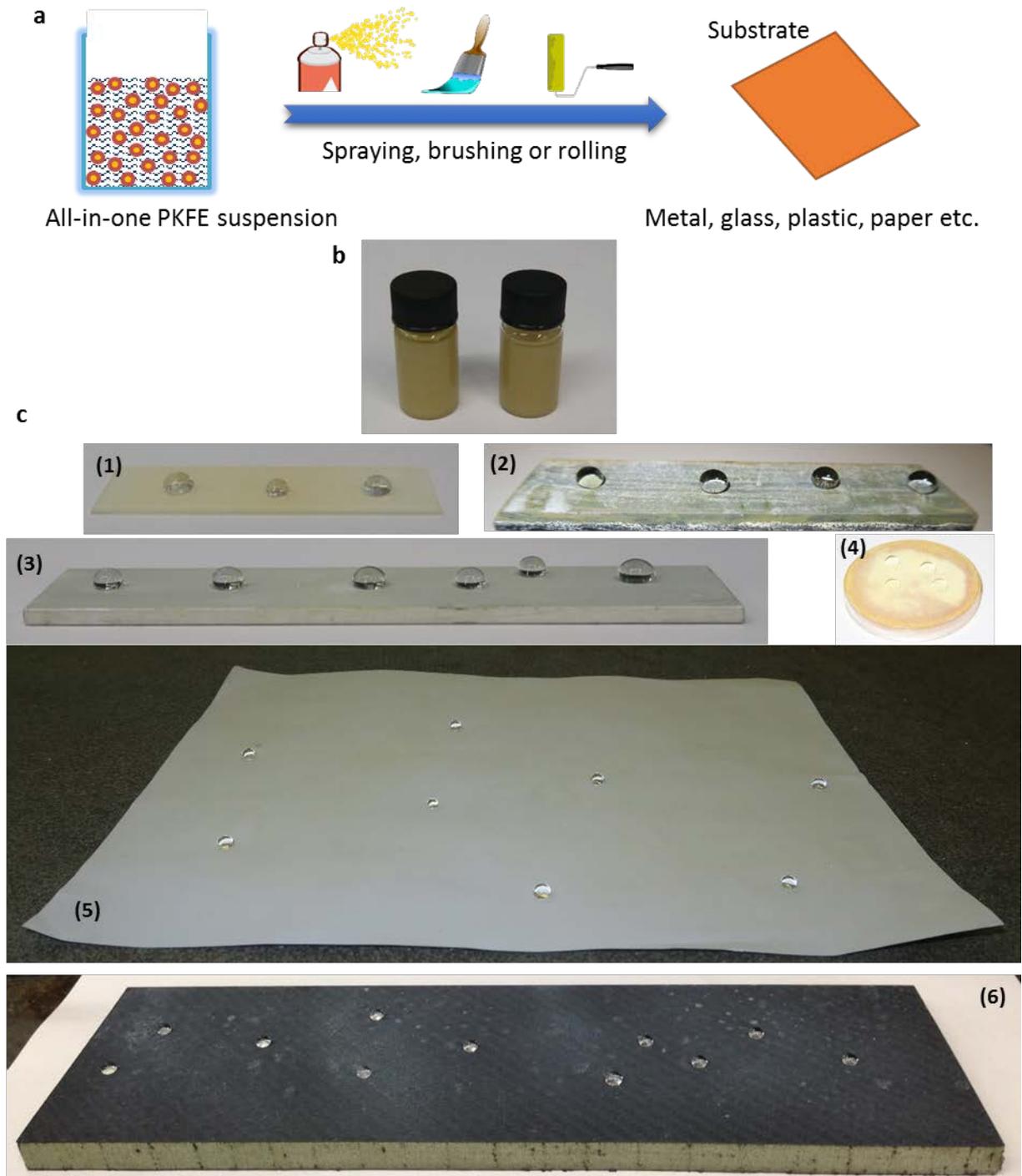
Supplementary Figure 2. PKFE coating application process. a, Schematic of all-in-one PKFE coating application via common scalable approaches such as spraying, brushing, rolling, etc. **b**, Picture of PKFE suspension as prepared (left vial) and stored in room environment for 30 days (right vial). **c**, Pictures of water repellent PKFE coating on a glass slide (75 mm × 25 mm) (1); 2 mm thick, steel plate (80 mm × 30 mm) (2); 2 mm thick, aluminium plate (120 mm × 25 mm) (3); back of polystyrene Petri dish (diameter 50 mm)(4); A4 printing paper (297 mm × 210 mm) (5); a sandwich panel with carbon fibre composite sheets and PVC foam core (350 mm × 200 mm) (6). No difference in wettability (θ_A and $\Delta\theta$) was observed, regardless of the substrate material and size. The A4 paper and the carbon fibre composite substrates are used to show scalability of coating fabrication process.
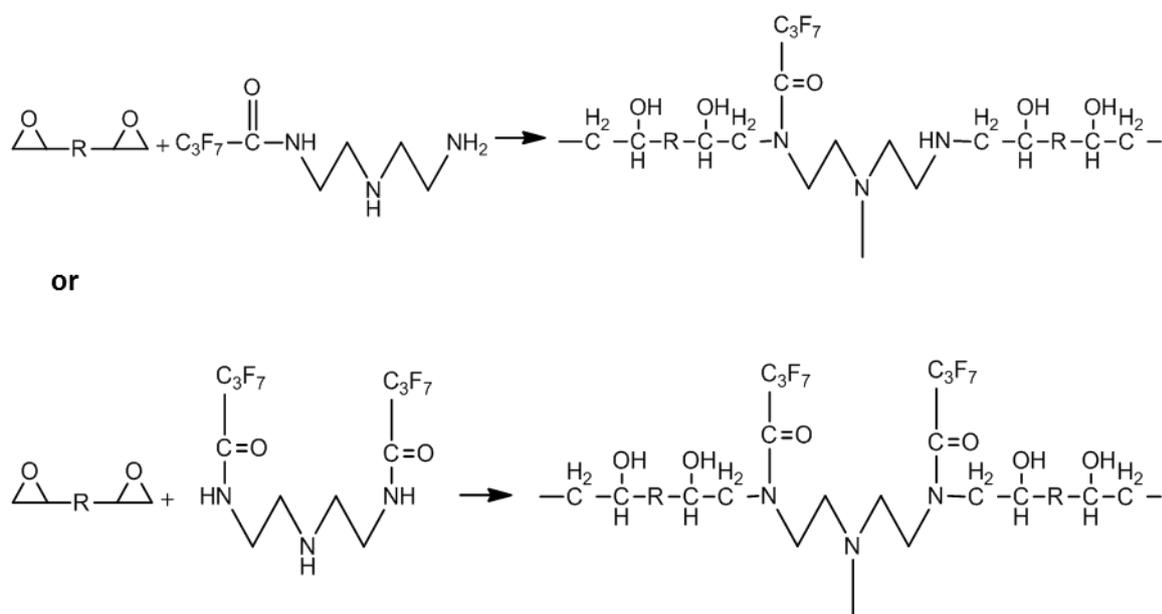

Supplementary Figure 3. Hardening mechanism of the epoxy in the PKFE coating.

Supplementary Note 1. Effect of nanoparticle concentration on mechanical robustness

PKFE nanocomposites with varying PTFE nanoparticle concentration were prepared in order to determine the optimal nanoparticle concentration required for the best possible mechanical

robustness while maintaining the excellent water repellency. Before determining its effect on mechanical characteristics, the change in the PKFE nanocomposite θ_A and $\Delta\theta$ with the PTFE concentration was explored and is plotted in Supplementary Figure 4. The substrates in this case were prepped by manual sandpaper (Grit: 240) roughening. Clearly superhydrophobicity is achieved at nanoparticle loadings exceeding 30 wt.%. For a smooth substrate such as a glass slide, superhydrophobicity was achieved at a higher particle loadings, above 60 wt.%.
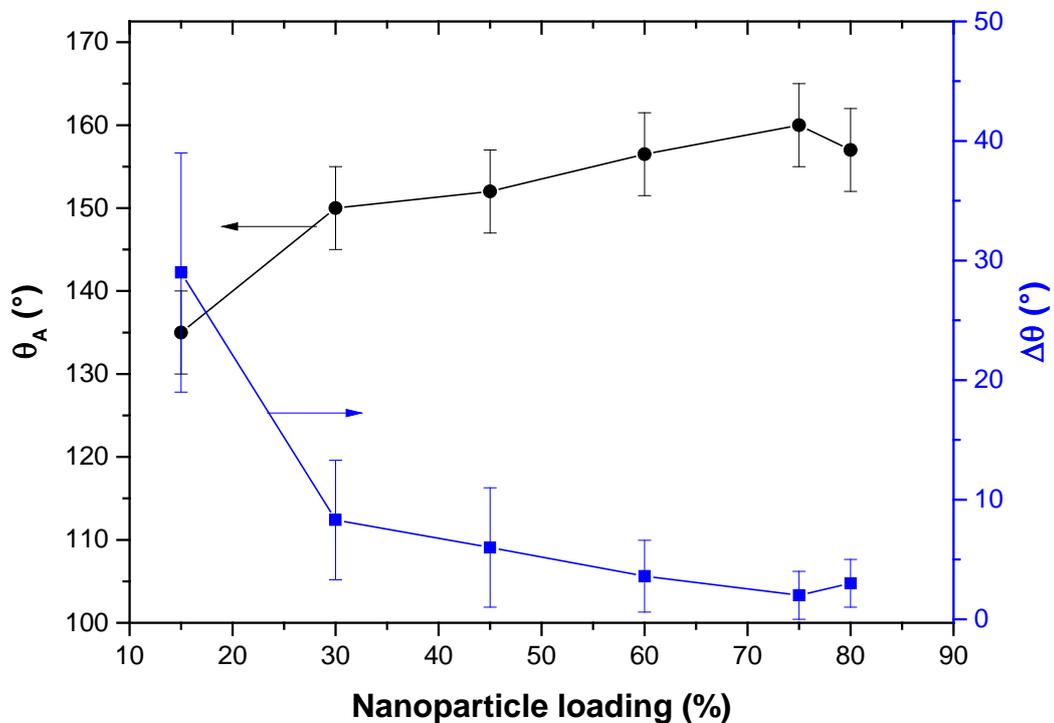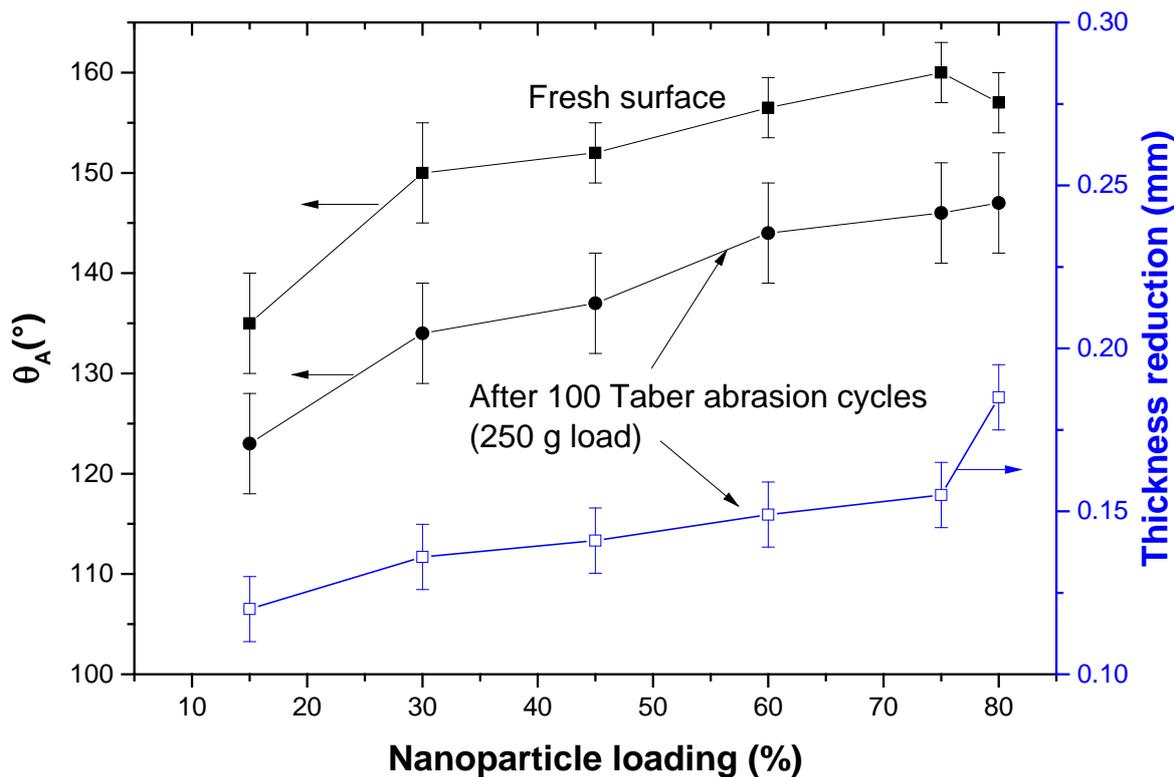

Supplementary Figure 4. Hydrophobicity of PKFE coating at different nanoparticle loadings. Error bars were obtained from distinct measurements on 3 different coating samples and at least at 3 different locations on each.

The effect of nanoparticle loading on the abrasion resistance of the nanocomposite coatings is presented in Supplementary Figure 5, which shows the coating θ_A before and after 100 cycles

of Taber abrasion (see Fig. 2c in the main manuscript and *cf.* Supplementary Figure 7 below).

The figure also plots the change in coating thickness after abrasion cycles. Clearly

mechanical abrasion leads to a decrease of θ_A. However, for the nanoparticle loadings greater

than 70 wt.%, a θ_A of ~146° is retained even after the 100 Taber abrasion cycles at 250 g

load. PTFE nanoparticles influence wear resistance of PKFE coating in two ways. On one

hand, due to its lubricity and softness, PTFE reduce the wear coefficient of epoxy resin[2] and

thereby helping to enhance the wear resistance of the PKFE nanocomposite coating. On the

other hand, as the PTFE nanoparticle loading goes up, the mechanical robustness should

decrease due to softness of PTFE and relatively weak interfacial bonding between PTFE

nanoparticles and the epoxy resin; the quality of nanoparticle dispersion also goes down at

very high particle content. These two effects are at odds with each other. Thus in

Supplementary Figure 3 we see that for nanoparticle loadings below 75 wt.%, the thickness

reduction of the nanocomposite after abrasion testing is fairly low, indicating that the wear

resistance of PKFE coating decreases only slightly with the nanoparticle content. However,

beyond 75 wt.%, the low interfacial bonding of the PTFE and epoxy and the softness of the

PTFE seem to start dominating and result in a sharp reduction in coating thickness with

abrasion (Supplementary Figure 3). Additionally, beyond 75 wt.% the poor dispersion quality

also resulted in visibly rough coatings; this is reflected in slight decrease in θ_A and increase in

$\Delta\theta$ with increase in particle loading from 75 wt.% to 80 wt.%. Overall, 75 wt.% particle

loading was optimal for both water repellency and wear resistance. Therefore, in this work,

unless mentioned otherwise, the PKFE coating were prepared with nanoparticle loading of 75

wt.%.

Supplementary Figure 5. Effect of nanoparticle loading on the hydrophobicity and wear resistance of the PKFE nanocomposite coating. Error bars were obtained from distinct measurements on 3 different coating samples and at least at 3 different locations on each.

Supplementary Note 2. Tape peel test

Supplementary Figure 6 shows the two kinds of tape peel tests employed; the cyclic tape application using a 4 kg steel roller and peel off (Supplementary Figure 6a). The Supplementary Figure 6b shows water droplets beaded up on the coatings after 30 tape peel cycles (c.f. θ_A and $\Delta\theta$ in Fig. 2b).
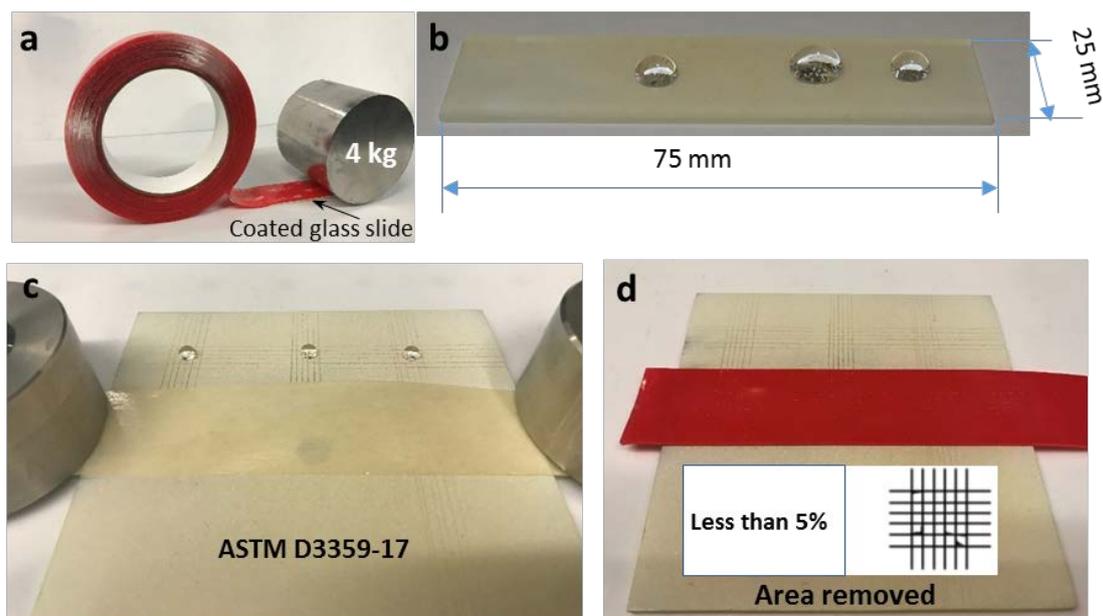
Supplementary Figure 6. Tape peel tests for assessing the adhesion of PKFE coating. a,
Application of a strong adhesive tape on to the PKFE coating. **b,** Water drops beaded up on the
surface and rolled off easily even after 30 tape peel cycles, the measured $\Delta\theta$ was less than 5° (see Fig.
2b). **c,** Outcome of cross hatch tape peel test performed on a PKFE coated glass plate (10 cm × 10 cm)
with Elcometer 99 tape in accordance with ASTM standard D3359-17, showing no coating peel off.
Water droplets still beaded up and rolled off easily from the tested region. **d,** Cross hatch test with the
VHB tape showing less than 5% damage. Both attest to strong adhesion of the PKFE coatings.

We also performed ASTM adhesion tests, using standard cross hatch engravings on the
coatings, followed by tape application and peel off (see Supplementary Figures 6c and 6d).
The new version of the ASTM standard (D3359-17) does not specify any specific tape and
suggests tapes with adhesion of steel value between 634 Nm^{-1} to 700 Nm^{-1}, which are lower
than 2,600 Nm^{-1} for the VHB tape used in repeated tape peel cycles above. Thus, for
completeness, we performed the cross hatch (ASTM) tape test using Elcometer 99 tape (with
adhesion to steel value of 642 Nm^{-1}) as well as the VHB tape. The Elcometer 99 tape did not
remove any coating (Supplementary Figure 6c), whereas none or less than 5% coatings was

removed on to the VHB tape (Supplementary Figure 6d). In each case, water droplets beaded up on the tested region (see Supplementary Figure 6c) and rolled off the substrate at an inclination of less than 5°.

Supplementary Note 3 Taber abrasion test

Abrasion tests were performed following ASTM D4060, using a Taber abrasion machine (see Fig. 2c and Supplementary Figure 7). The Taber machine uses two loaded abrasive wheels against which the coated sample is rubbed using a rotating platform (Supplementary Figure 7a). The abrasion test samples comprised of coated, 6 mm thick, 10 cm × 10 cm glass plates. A 6 mm diameter hole was drilled in the centre of the glass plate to help secure it on the rotary platform of the Taber machine (Supplementary Figure 7b). Following the ASTM standard, one rotation of the substrate was counted as one cycle. The coatings' advancing and receding contact angles as well as thickness were measured periodically and are all presented in Fig. 2d. After 100 cycles of abrasion, water drops still showed very high θ_A on the coating (see Supplementary Figure 7c and Fig. 2d). Any abrasive particles or coating fragments appearing on the PKFE surface during abrasion tests could be rinsed away easily with tap water due to self-cleaning property (i.e. so called *Lotus leaf effect*[3], also marked by low contact angle hysteresis) of coatings. The Taber abrasion test was also used to compare the performance of PKFE coatings against four different state-of-the-art coatings in Supplementary Figure 14b.
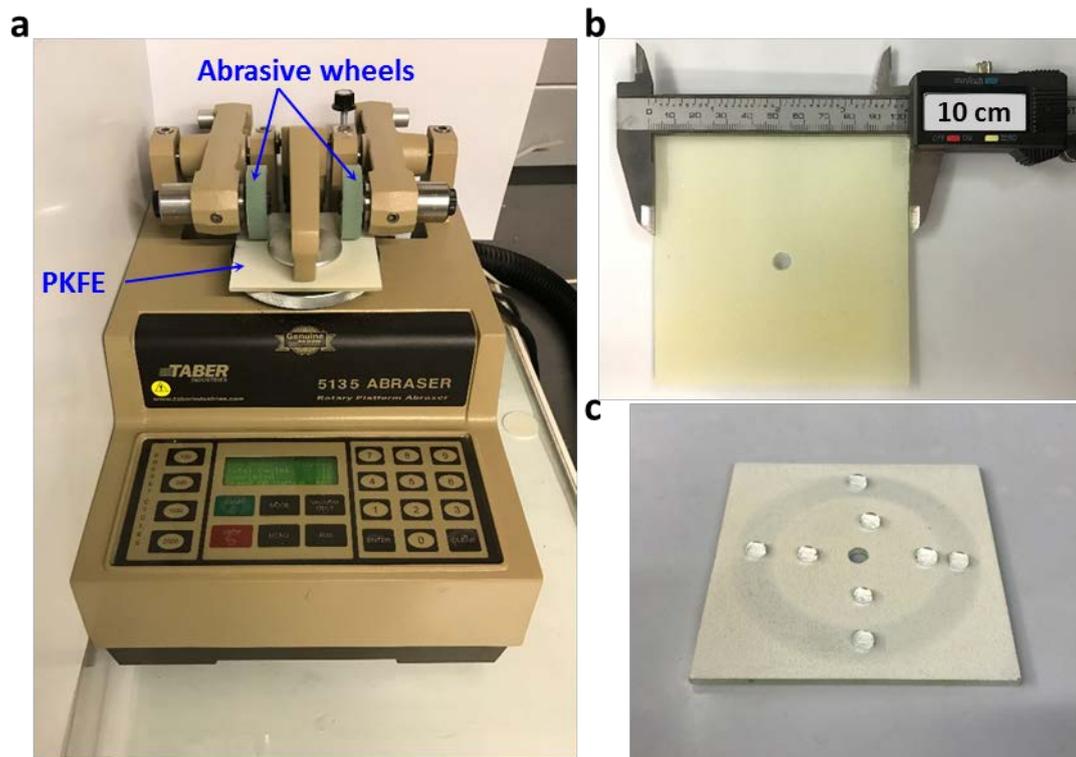
Supplementary Figure 7. Abrasion resistance of the PKFE coating. a, Picture of Taber abrasion machine featuring the abrasive wheels and mounted PKFE coated glass plate. **b,** A PKFE coated, 6 mm thick glass plate with central hole for mounting on the Taber machine. **c,** Water drops beaded up on the PKFE coating even after 100 abrasion cycles and could easily be rolled off. The circular abraded region is also clearly visible due to reduction of coating thickness from abrasive wear.

Supplementary Note 4. Droplet impact test

For testing liquid impalement resistance of the PKFE coatings, we used water drop and jet impact tests. The drop impact tests were performed by releasing individual water drops from a certain height to enable gravity led acceleration of the drops and achieve different impact speeds. Supplementary Movie 1 shows the drop impacts at different speeds. Supplementary Figure 8 captures the key features of droplet impact process at three different speeds. At low speed (e.g. 1 ms^{-1} in Supplementary Figure 8), the impact is characterised by droplet spreading, recoil and complete bounce off from the surface. At higher speeds the impact We_l

Confidential

is high enough for the droplet to splash and atomize. As the Supplementary Figure 8 shows, at ~4.6 ms^{-1} the droplet atomize upon impact and the resulting droplet fragments spend much less time on the substrate; down to ~8.0 ms compared to 15.3 ms at ~1 ms^{-1}, i.e., a more than 50% reduction in contact time. The high liquid mobility and reduction in contact time is beneficial when designing superhydrophobic surfaces for cold droplet impact resistance needed in anti-icing applications[4]. Note that the contact time is counted from the start of drop contact with the surface (i.e. starting with the second image in each row in Supplementary Figure 8).
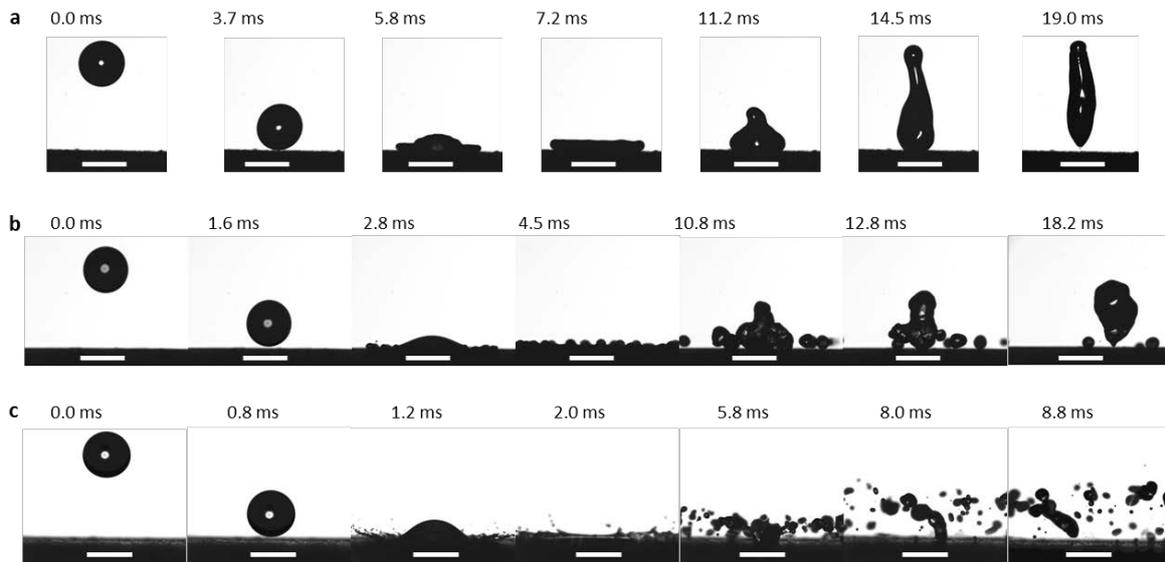

Supplementary Figure 8. Water droplets bouncing and atomizing upon impact on the PKFE coating at different speeds. a, Impact speed ~1.0 ms^{-1}, water droplet does not break up. **b,** Impact speed ~2.0 ms^{-1}, water droplet starts to break up and the main body of the droplet bounces off, but few very small water droplets scatter on the surface. These drops were highly mobile on the surface. **c,** Impact speed ~4.6 ms^{-1}, water droplet atomizes (breaks up) upon impact and its substrate contact time is reduced quite dramatically. Note the substrate contact is made in the second image in each row. Thus, contact time (*starting from second image in each row*) is ~8.0 ms at the impact speed of ~4.6 m/s as opposed to from ~15.3 ms for ~1 ms^{-1}. All scale bars, 2.5 mm.

Supplementary Note 5. Jet impact test

Maximum attainable drop speed in gravity enabled acceleration is limited by terminal velocity. Thus for higher speed liquid impact tests, we employed water jets. The setup shown schematically in Supplementary Figure 9 was used to obtain stable and controllable water jet with high speed. A high pressure nitrogen gas cylinder connected to an electronic pressure valve was used to force water through a nozzle connected to a piston (a needle/syringe assembly). With a nozzle diameter of 2.5 mm, the ensuing water jet could drain the cylinder volume of 4 ml in ~380 ms – recorded using the high speed camera. This is equivalent to an average jet speed of 21 ms^{-1} (We_l ~15,000). The water jet diameter was ~2.5 mm as well. However, due to system transients, upon application of pressure control signal on the electronic control valve, the gas back pressure on the piston will ramp up to the maximum 11 bar. This transient process should enable a time dependent rise in jet speed before levelling off to a steady rate corresponding to the maximum applied pressure. To unravel this transience, we recorded the motion of the piston/water interface inside the cylinder during typical jet impact process using the high speed camera. The motion of the piston could be used to determine the jet speeds through simple mass conservation and knowledge of cylinder and nozzle diameters. Thus, if in time Dt the piston in the cylinder moves by a distance Dh, we can write $\pi D^2 Dh/4 = \pi d^2 VDt/4$, where D is the cylinder diameter, d the nozzle (jet) diameter and V the jet speed. The resulting maximum jet speed – determined by averaging the maximum impact speeds in different tests – was 35.1 ms^{-1} (Supplementary Figure 10), with the corresponding We_l ~43,000. The surface showed no signs of liquid impalement. This is the highest We_l achieved on a superhydrophobic surfaces to the best of our knowledge. After water jet impact, small water droplet is observed to bounce off from the impact spot (see

bottom row images in Supplementary Figure 11), indicating the intactness of water

repellency even after ~35 ms^{-1} water jet impact (Supplementary Movie 6).
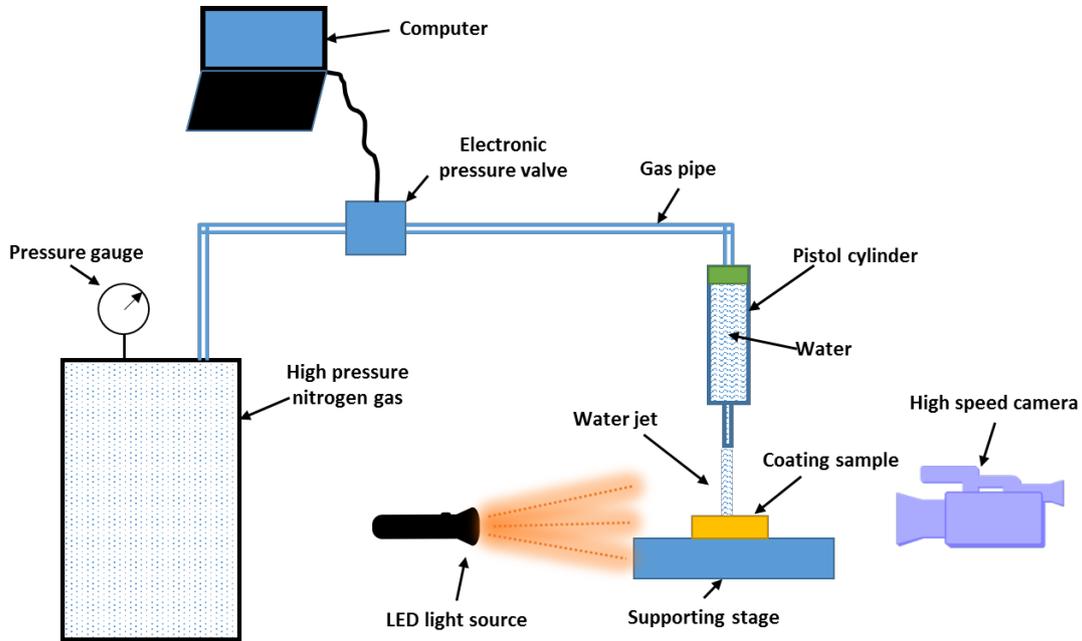
Supplementary Figure 9. Schematic of water jet impact setup.
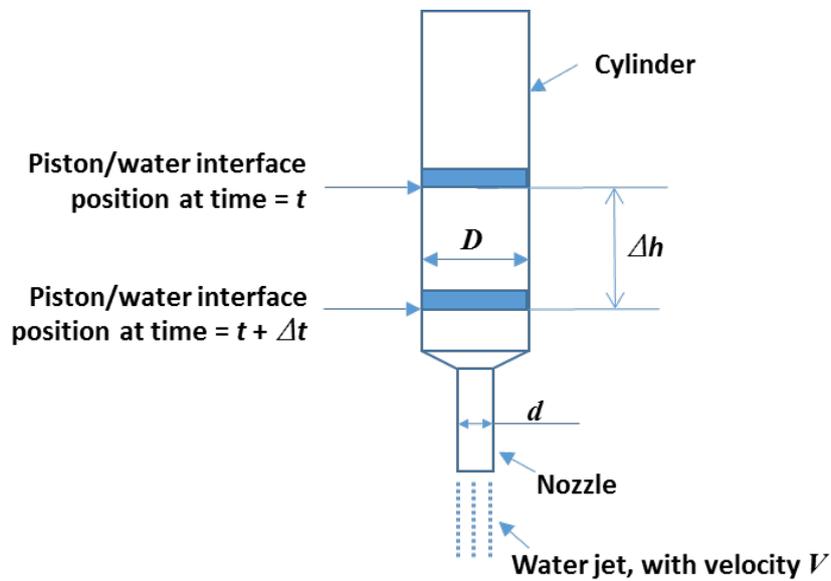
Supplementary Figure 10. Water jet velocity calculation by recording the piston/water

interface motion. High speed of camera was used to record the pneumatically actuated movement of

piston/water interface from position 1 (at time = *t*) to position 2 (at time = *t* + *Dt*). The volume of ejected water in time *Dt* could then be calculated using the amount of the piston/water interface motion (*Dh*) and the cylinder diameter (*D*). Mass conservation was then used to determine the jet velocity *V*.
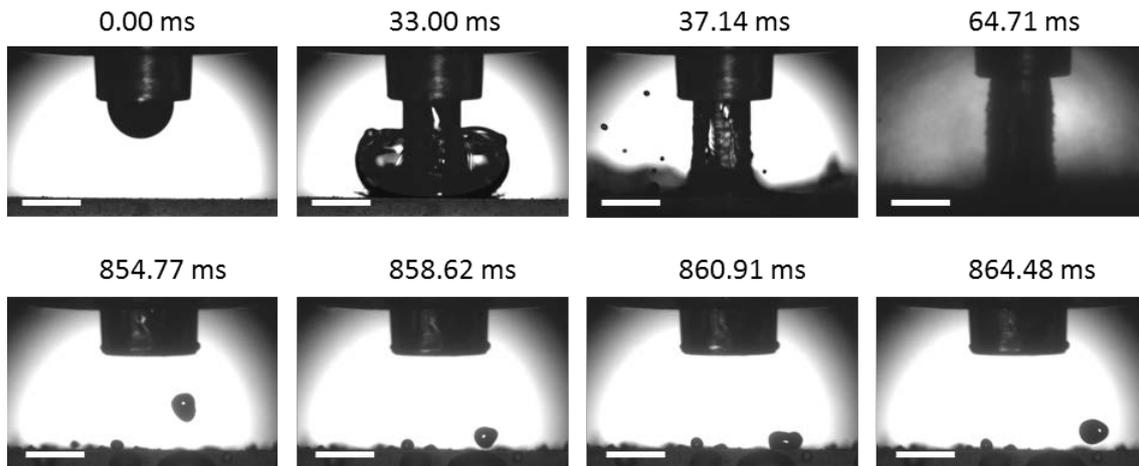
Supplementary Figure 11. Highest jet impact speed tested on a superhydrophobic surface. The top row images capture the jet impact test. The bottom row images capture a remaining water droplet from the nozzle – *well after the jet impact test* – impacting on the substrate and bouncing off completely, indicating an absence of surface damage. Our setup (Supplementary Figure 9) enabled testing of PKFE nanocomposite coatings up to a highest jet impact speed of 35.1 ms^{-1} with the corresponding We_l ~43,000 – the latter (We_l) points to the highest ever impalement resistance reported. After the water jet impact test, the surface showed no signs of damage or impalement by liquid. This was also tested by water drop roll-off tests and measuring the restitution coefficient of a drop impacting at the location of jet impact.

To ascertain a lack of liquid impalement into the surface texture, firstly we tested droplet impact and complete rebound at the location of jet impact. The result of this drop impact test

is presented in case 4 in Fig. 2h of the main paper. Additionally, low speed droplet impact tests were used to determine the coefficient of restitution before and after the jet impact test. In analogy with a rubber ball bouncing off after impact on a rigid substrate, the restitution coefficient for a droplet bouncing off on a surface is defined as the ratio of droplet speed at the point of lift-off from the substrate to the drop speed right before impact[5]. Post-impact the drop undergoing inertial spreading, followed by recoil and total lift-off. High speed videos of drop impact on the PKFE coating were digitised and processed by Matlab® to obtain the impact and lift-off velocity for the drop centre of mass. The results are plotted in Supplementary Figure 12 below, which shows restitution coefficients measured on the fresh PKFE coatings as well as after high speed jet impact (Supplementary Movie 6 and Supplementary Figure 11). Note that these experiments were performed with slightly smaller drops (diameter ~1.9 mm) and at low impact speeds to avoid drop fluctuations, which affect the restitution coefficient measurements[5,6,7]. The error bars are obtained from three different impact tests at any given speed. The error bars are larger at low impact speed due to greater positional errors at low impact speeds, as also reported in the original experiments by Richard *et al.* [5,6]. At progressively higher speeds the restitutions coefficient for both fresh and post-impact PKFE coatings seem to stabilize at ~0.9. Such a high value of restitution coefficient corresponds to low adhesion of the surface towards the droplet and a lack of liquid impalement during jet impact, as observed above. The Supplementary Figure 12 also shows two horizontal lines, at restitution coefficients of 0.91 and 0.85. These correspond to loss-less, spherical (0.91) or elongated (cylindrical, 0.85) lift-off of the droplet after impact[5].
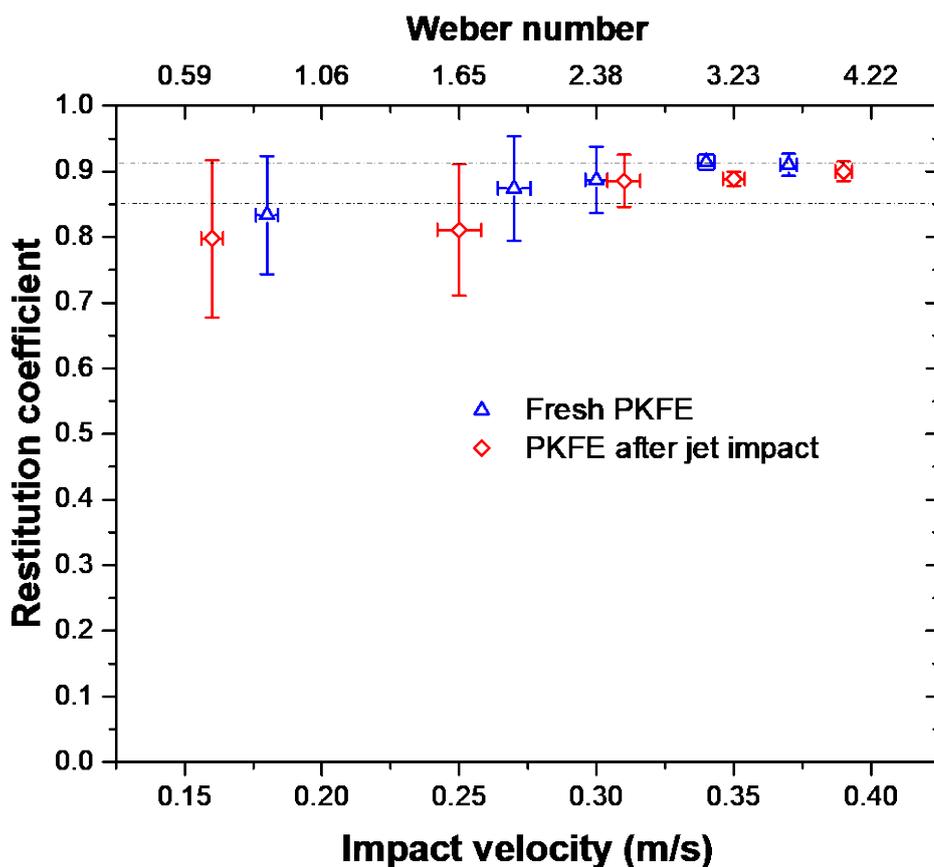
Supplementary Figure 12. Restitution coefficient on PKFE coatings. The restitution coefficient measured before and after high speed jet impact test, plotted as a function of drop impact speeds (the corresponding Weber numbers are plotted as top horizontal axis). Larger error bars at low speeds result from position errors in image processing which are greater at low speed. At higher speeds (>0.3 ms^{-1}) the restitution coefficient before and after jet impact is indistinguishable, reflecting a lack of liquid impalement into the PKFE surface texture. Error bars were obtained from distinct measurements on 3 different coating samples and at least at 3 different locations on each.

Supplementary Note 6. Role of coating flexibility in impalement resistance

Impalement of the liquid meniscus into hydrophobic surface texture is resisted by capillary pressure, which can be expressed as

$$P_c = \frac{2\gamma_{SG}\cos\theta}{r_p}$$

(Supplementary Eq. 1)

where r_p is the effective pore radius of the surface texture[4]. The meniscus impalement is favoured by dynamic and water hammer pressures due to the liquid impact[4]. The dynamic pressure can be expressed as

$$P_d = \frac{1}{2}\rho_l V^2$$

(Supplementary Eq. 2)

The water hammer pressure originates from compressibility of liquid and can be written as[4]

$$P_{wh} = kZ_e V$$

(Supplementary Eq. 3)

where k is an empirical constant and Z_e is the effective acoustic impedance of the liquid and substrate (coating) system and can be written as

$$Z_e = \frac{\rho_l c_l \rho_s c_s}{\rho_l c_l + \rho_s c_s} = \frac{Z_l Z_s}{Z_l + Z_s}$$
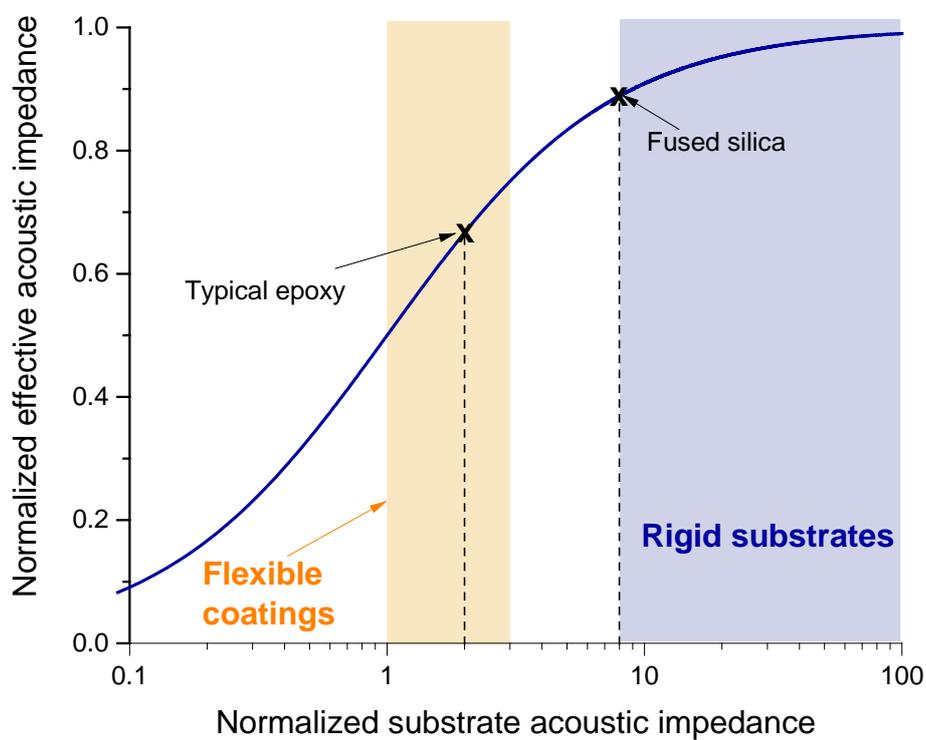
(Supplementary Eq. 4)

The effective acoustic impedance is a combination of liquid and substrate acoustic impedances, Z_l and Z_s, respectively. Supplementary Eq. 4 uses the definition of acoustic impedance, which for any material is a product of its density, ρ, and speed of sound through it, c. The subscripts l and s denote the liquid and the substrate respectively. Typically, water hammer pressure is much larger than dynamic pressure and, therefore, controls the liquid meniscus penetration in to the surface texture. For further insight, Supplementary Eq. 4 can be written in a normalized form as

$$Z_e/Z_l = \frac{\rho_s c_s}{\rho_l c_l + \rho_s c_s} = \frac{Z_s/Z_l}{1 + Z_s/Z_l}$$

(Supplementary Eq. 5)

For rigid substrates (i.e. $Z_l \ll Z_s$); thus, the right hand side of Supplementary Eq. 5 becomes unity and we can write the water hammer pressure to be

$$P_{wh} = kZ_l V = k\rho_l c_l V$$

(Supplementary Eq. 6)

Supplementary Eq. 6 is often used in the literature. However, for light and flexible substrates/coatings, the approximation of Z_l being much smaller than Z_s will break down. To illustrate this issue, the normalized effective acoustic impedance (Z_e/Z_l from Supplementary Eq. 5) is plotted in Supplementary Figure 13 against the normalized substrate acoustic impedance (Z_s/Z_l) and zones of flexible and rigid substrates are demarked in orange and blue colours (based on data from[8]). Clearly for flexible substrates and coatings, the effective impedance is lower than that for rigid substrates – this will reduce the magnitude of P_{wh}.

Supplementary Figure 13. Variation in normalized effective acoustic impedance with change in the normalized substrate acoustic impedance. Flexible substrates or coatings clearly have lower effective acoustic impedance, which will reduce the peak water hammer pressure on these substrates.

Near room temperature, as in our experiments, for water Z_l ~1.5 MRayl, for epoxy Z_s ~3 MRayl, for PTFE ~3 MRayl and that for fused silica ~12 MRayl (data from[8]). In Supplementary Figure 11 we have marked epoxy (similar to our coating) and fused silica as a

typical rigid substrate. The effective normalized impedances for epoxy and fused silica (see Supplementary Figure 13) are 0.67 and 0.89, respectively. The difference is as much as ~25%. Note that from Supplementary Eq. 3 since the P_{wh} is directly related to Z_e, this amounts to a corresponding reduction in water hammer pressure by same percentage. Here we have selected fused silica as a conservative example. The Z_s of aluminium – material of wide usage in aerospace industry – is similar to that of fused silica. Other inorganic materials such as alumina, titania etc. and rigid metal and alloys such as titanium, stainless steel have much larger value of Z_s; the water hammer pressure will correspondingly be even higher on these substrates. Therefore, the choice of flexible all-organic coatings (see Supplementary Movie 7) with good mechanical integrity and robustness (see Fig. 2) is expected to contribute favourably to impalement resistance, as is demonstrated by our coatings.

Supplementary Note 7. Comparison with immiscible oil infused surfaces

Use of Krytox (perfluoropolyether) in our PKFE formulation may raise comparison with recently proposed oil infused liquid repellent surfaces, where immiscibility of oil with water is exploited to obtain low drop sliding angles[9]. Supplementary Movie 8 compares the droplet motion on a Krytox infused surface and our PKFE coating. We obtained the Krytox infused part by gently dropping a few drops of Krytox on our coatings. This resulted in hemi-wicking of Krytox and formed the Krytox infused wet part of the slide in Supplementary Movie 8. The movie clearly shows much faster droplet motion on the PKFE coating compared to the Krytox infused part (i.e. the wet part) of the slide, confirming a much higher drop adhesion with the Krytox infused section. The key difference is that, despite both surfaces being soft, the adhesion of water drops on an oil infused surface is controlled by the oil viscosity[33]. Therefore, our strategy to blend Krytox in the coatings formulation rather than infusing the Krytox *a posteriori* has clear advantages.

Supplementary Note 8. Comparison with existing sprayable superhydrophobic coatings

Here we compare the performance of PKFE coatings against four different state-of-the-art, spray coated superhydrophobic surfaces. The first is a nanocomposite coating comprising of carbon black (CB) nanoparticles dispersed in a fluoroacrylic copolymer (Capstone ST-100® from DuPont). The coating was prepared following the protocol reported previously[10], with equal weight fractions of CB and Capstone in the nanocomposite. In Supplementary Figure 14, presenting the comparative data, this coating is denoted as Capstone-CB. We also included three different commercial coatings in our comparison: NTT-AT HIREC 450 from Japan, Ultra-Ever Dry and NeverWet, which were all prepared by spraying, in accordance with the supplier's guidance notes. Ultra-Ever Dry and NeverWet are two-part coatings, i.e., they use a primer for adhesion improvement. This is in contrast to PKFE, Capstone-CB and HIREC 450, which are each one part sprayable formulations and thereby offer an advantage in terms of field application of these coatings. The comparative data presented in Supplementary Figure 14 were obtained by following the test protocols outlined in the Methods section of the main paper; at least three samples were tested in each case. Firstly, Supplementary Figure 14a shows the number of repeated tape peeling cycles that a coating could sustain before the contact angle hysteresis ($\Delta\theta$) increasing beyond 10°, which is taken are a comparative metric since this is the limit of self-cleaning property for superhydrophobic surfaces. Whereas the state-of-the-art coating survive a mean of 5-7 cycles, PKFE coatings lasted 30 cycles, marking a 4-6 fold improvement. We note that the Ultra-Ever Dry started showing signs of physical damage after 5 peeling cycles. Next, Taber abrasion test was used as the second mechanical robustness test. As shown in Supplementary Figure 14b, PKFE

coatings survived 80 abrasion cycles at a load of 250 g, which was nearly twice as good as the Ultra-Ever Dry coatings that lasted a mean of 45 abrasion cycles. The Supplementary Figure 14c shows the result of NaOH compatibility tests. Even in this case whereas PKFE maintained superhydrophobicity ($\Delta\theta < 10°$) after 12 h of 1M NaOH exposure, all commercial coatings got damaged in couple of hours at most; HIREC 450 fell apart in 5 minutes and the Capstone-CB in a mean time of 1 h. Thus, PKFE coatings seem to have much better chemical robustness; demonstrating nearly one order of magnitude better resistance to NaOH exposure. The results of jet impact tests are presented in Supplementary Figure 14d. The figure reports the maximum jet speed (hatched bars) tested and the corresponding We_l (filled bars). Note the green arrow above the bars for PKFE coating is meant to indicate that we did not reach impalement for PKFE coatings in our setup, as indicated in the main paper. For the state-of-the-art coatings, the jets were of 0.25 mm diameter and each of these coatings showed liquid impalement beyond a critical jet speed. The liquid impalement was tested by placing a droplet at the location of impact and assessing whether the droplet rolled off at any tilt angle. The PKFE coatings were also tested repeatedly with jets of 0.25 mm without showing signs of impalement. In Supplementary Figure 14d, the reported jet speed and We_l for the PKFE coatings was obtained with a 2.5 mm diameter jet, which corresponded to a maximum tested We_l of ~43,000, *without showing impalement*. The inset shows the critical We_l's achieved for the other coatings; PKFE coating clearly demonstrates well over an order of magnitude improvement.
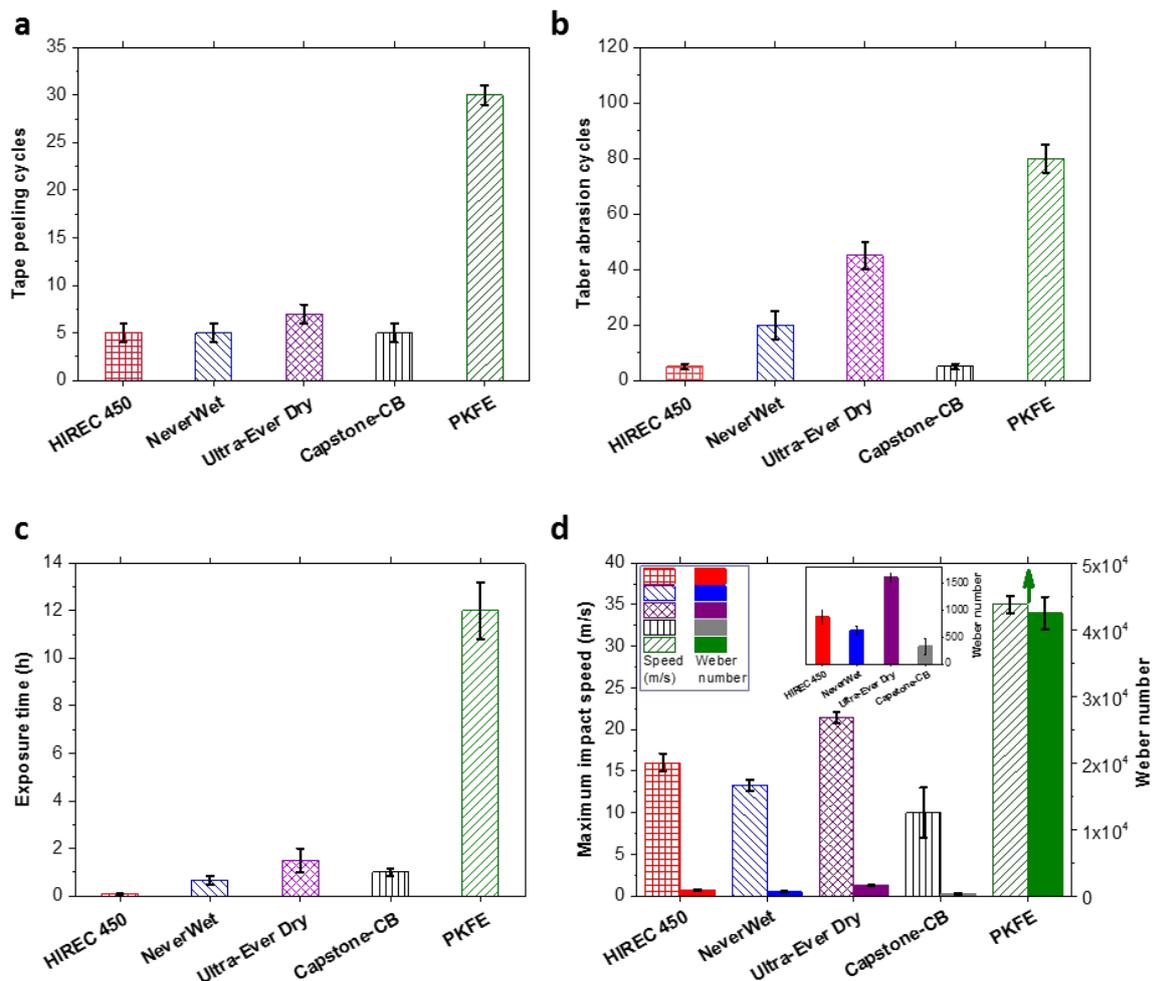
Supplementary Figure 14. Comparing PKFE robustness against several state-of-the-art coatings.
HIREC 450 and Capstone-CB are one part coatings just as PKFE, whereas NeverWet and Ultra-Ever
Dry are two part coatings, requiring a primer. HIREC 450, NeverWet and Ultra-Ever Dry are
commercial coatings and Capstone-CB (with 1:1 CB to Capstone) is from a previous work. **a,** Tape
peel cycles sustained by coatings before reaching a contact angle hysteresis ($\varDelta\theta$) beyond 10°; PKFE
performance is 4-6 times better. **b**, Number of Taber abrasion cycles with a loading of 250 g, survived
before $\varDelta\theta$ increasing beyond 10°; PKFE is about twice as good compared to the next best coating. **c,**
results of NaOH exposure tests, with PKFE showing nearly one order of magnitude better resistance.
d, Jet impalement tests show critical impalement speeds and We_l for other coatings (see also the inset),
whereas PKFE remains dry (indicated by the green arrow) up to maximum attainable jet speed and We
in our setup; demonstrating well over an order of magnitude improvement. Error bars were obtained

from distinct measurements on 3 different coating samples and at least at 3 different locations on each.

Supplementary References

1   Dumouchel, C. On the experimental investigation on primary atomization of liquid streams. *Exp. Fluids* **45**, 371-422, doi:10.1007/s00348-008-0526-0 (2008).

2   McCook, N. L. et al. Wear resistant solid lubricant coating made from PTFE and epoxy. Tribol. Lett. 18, 119-124, doi:10.1007/s11249-004-1766-7 (2005).

3   Feng, X. J. & Jiang, L. Design and creation of superwetting/antiwetting surfaces. Adv. Mater. 18, 3063-3078, doi:10.1002/adma.200501961 (2006).

4   Maitra, T. et al. On the nanoengineering of superhydrophobic and impalement resistant surface textures below the freezing temperature. Nano Lett. 14, 172-182, doi:10.1021/nl4037092 (2014).

5   Richard, D. & Quere, D. Bouncing water drops. Europhys. Lett. 50, 769-775, doi:10.1209/epl/i2000-00547-6 (2000).

6   Richard, D., Clanet, C. & Quere, D. Surface phenomena: Contact time of a bouncing drop. Nature 417, 811-811, doi:10.1038/417811a (2002).

7   Schutzius, T. M. et al. Spontaneous droplet trampolining on rigid superhydrophobic surfaces. Nature 527, 82-85, doi:10.1038/nature15738 (2015).

8   http://www.ondacorp.com/tecref_acoustictable.shtml, (2003).

9   Wong, T. S. et al. Bioinspired self-repairing slippery surfaces with pressure-stable omniphobicity. Nature 477, 443-447, doi:10.1038/nature10447 (2011).

10   Asthana, A., Maitra, T., Buchel, R., Tiwari, M. K. & Poulikakos, D. Multifunctional superhydrophobic polymer/carbon nanocomposites: graphene, carbon nanotubes, or carbon black? ACS Appl. Mater. Inter. 6, 8859-8867, doi:10.1021/am501649w (2014).